

UNCLASSIFIED

AD NUMBER
ADB089870
NEW LIMITATION CHANGE
TO Approved for public release, distribution unlimited
FROM Distribution authorized to U.S. Gov't. agencies and their contractors; Specific Authority; SEP 1984. Other requests shall be referred to Rome Air Development Center, AFSC, Griffiss AFB, NY.
AUTHORITY
RL USAF ltr, 18 Jun 1992

THIS PAGE IS UNCLASSIFIED

AD-B089 870

RADC-TR-84-61

In-House Report

September 1984



2

DETECTION PERFORMANCE FOR OVER RESOLVED TARGETS

Vincent C. Vannicola and Kenneth G. Hillman

*DISTRIBUTION LIMITED TO U.S. GOVERNMENT AGENCIES AND THEIR CONTRACTORS; SPECIFIC
AUTHORITY, PUBLIC LAW 98-94; Sep 84. OTHER REQUESTS FOR THIS DOCUMENT SHALL BE REFERRED
TO RADC (OCTS), GRIFFISS AFB, NY 13441-5700.*

INFORMATION SUBJECT TO EXPORT CONTROL LAWS

This document may contain information subject to the International Traffic In Arms Regulation (ITAR) or the Export Administration Regulation (EAR) of 1979 which may not be exported, released, or disclosed to foreign nationals inside or outside the United States without first obtaining an export license. A violation of the ITAR or EAR may be subject to a penalty of up to 10 years imprisonment and a fine of \$100,000 under 22 U.S.C. 2778 or Section 2410 of the Export Administration Act of 1979. Include this notice with any reproduced portion of this document.

**ROME AIR DEVELOPMENT CENTER
Air Force Systems Command
Griffiss Air Force Base, NY 13441-5700**

DTIC
UNCLASSIFIED
1985




B

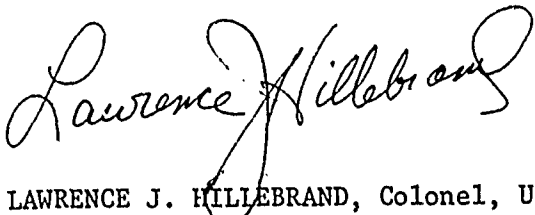
223 FILE COPY

RADC-TR-84-61 has been reviewed and is approved for publication.

APPROVED:


FRED J. DEMMA
Chief, Surveillance Technology Branch
Surveillance Division

APPROVED:


LAWRENCE J. HILLEBRAND, Colonel, USAF
Chief, Surveillance Division

FOR THE COMMANDER:



JOHN A. RITZ
Acting Chief, Plans Office

If your address has changed or if you wish to be removed from the RADC mailing list, or if the addressee is no longer employed by your organization, please notify RADC (OCTS) Griffiss AFB NY 13441. This will assist us in maintaining a current mailing list.

Do not return copies of this report unless contractual obligations or notices on a specific document requires that it be returned.

UNCLASSIFIED

SECURITY CLASSIFICATION OF THIS PAGE

REPORT DOCUMENTATION PAGE				
1a. REPORT SECURITY CLASSIFICATION UNCLASSIFIED		1b. RESTRICTIVE MARKINGS N/A		
2a. SECURITY CLASSIFICATION AUTHORITY N/A		3. DISTRIBUTION/AVAILABILITY OF REPORT U.S. Govt agencies and their contractors; specific authority, Public Law 98-94; Sep 84. Other requests RADC (OCTS) GAFB NY 13441-5700.		
2b. DECLASSIFICATION/DOWNGRADING SCHEDULE N/A				
4. PERFORMING ORGANIZATION REPORT NUMBER(S) N/A		5. MONITORING ORGANIZATION REPORT NUMBER(S) RADC-TR-84-61		
6a. NAME OF PERFORMING ORGANIZATION Rome Air Development Center	6b. OFFICE SYMBOL (If applicable) OCTS	7a. NAME OF MONITORING ORGANIZATION Rome Air Development Center		
6c. ADDRESS (City, State and ZIP Code) Griffiss AFB NY 13441		7b. ADDRESS (City, State and ZIP Code) Griffiss AFB NY 13441		
8a. NAME OF FUNDING/SPONSORING ORGANIZATION AFOSR	8b. OFFICE SYMBOL (If applicable)	9. PROCUREMENT INSTRUMENT IDENTIFICATION NUMBER N/A		
9c. ADDRESS (City, State and ZIP Code) Bolling AFB Wash DC 20332		10. SOURCE OF FUNDING NOS.		
		PROGRAM ELEMENT NO. 61102F	PROJECT NO. 2305	TASK NO. J8
		WORK UNIT NO. 17		
11. TITLE (Include Security Classification) DETECTION PERFORMANCE FOR OVER RESOLVED TARGETS				
12. PERSONAL AUTHOR(S) Vincent C. Vannicola, Kenneth G. Hillman				
13a. TYPE OF REPORT In-House	13b. TIME COVERED FROM Mar 83 to Feb 84	14. DATE OF REPORT (Yr., Mo., Day) September 1984	15. PAGE COUNT 64	
16. SUPPLEMENTARY NOTATION N/A				
17. COSATI CODES		18. SUBJECT TERMS (Continue on reverse if necessary and identify by block number)		
FIELD	GROUP	SUB. GR.		
17	09	Detection		
09	04	High Resolution		
		Radar		
19. ABSTRACT (Continue on reverse if necessary and identify by block number)				
<p>This report is an investigation into how detection probabilities of scatterers are affected as radar range resolution divides the target into multiple scatterers. The work is applied to several scatterer models: the constant amplitude, Rayleigh, and dominant plus Rayleigh scatterers.</p> <p>Throughout the treatment, detection probability is plotted against signal-to-noise ratio with the degree of resolution as a parameter. All other conditions such as total target cross section, false alarm probability, and number of pulses are held constant for each set of curves.</p> <p>In this work, detection is based on at least one threshold crossing out of the M range cells of which the target has been resolved. As M increased, improvements in detection performance were noted only at high signal levels for a limited variety of scatterers: the single pulse Rayleigh and dominant plus Rayleigh, the multiple pulse slow (Cont'd)</p>				
20. DISTRIBUTION/AVAILABILITY OF ABSTRACT UNCLASSIFIED/UNLIMITED <input checked="" type="checkbox"/> SAME AS RPT. <input type="checkbox"/> DTIC USERS <input type="checkbox"/>		21. ABSTRACT SECURITY CLASSIFICATION UNCLASSIFIED		
22a. NAME OF RESPONSIBLE INDIVIDUAL VINCENT C. VANNICOLA		22b. TELEPHONE NUMBER (Include Area Code) (315) 330-4437	22c. OFFICE SYMBOL RADC (OCTS)	

DD FORM 1473, 83 APR

EDITION OF 1 JAN 73 IS OBSOLETE.

UNCLASSIFIED
SECURITY CLASSIFICATION OF THIS PAGE

UNCLASSIFIED

SECURITY CLASSIFICATION OF THIS PAGE

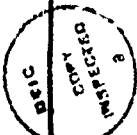
fluctuating Rayleigh and dominant plus Rayleigh. All other targets showed a loss over all signal-to-noise ratios as the number of resolution cells was increased. It is shown that an improvement occurs with increasing resolution, so long as the estimated cross section in each range cell has a large error variance. This holds for single as well as multiple pulse waveforms of which the pulses represent dependent samples (slow fluctuating target).

Analogous effects of distributed clutter on false alarm count are discussed in the concluding remarks.

Additional keywords: high resolution, charts, mathematical models, computations,

DTIC
ELECTE
MAR 7 1985
B

Accession For	
NTIS GRA&I	<input type="checkbox"/>
DTIC TAB	<input checked="" type="checkbox"/>
Unannounced	<input type="checkbox"/>
Justification	
By	
Distribution/	
Availability Codes	
Dist	Avail and/or Special
C-2	



UNCLASSIFIED

SECURITY CLASSIFICATION OF THIS PAGE

TABLE OF CONTENTS

I. Introduction	1
II. Approach	4
III. False Alarm And Threshold Determination	5
IV. Decision Rule for Scatterer Detection	6
V. Detection Probability - Target of M Range Cells	9
A. Single Pulse Waveform ($N = 1$)	9
1) Constant Amplitude Scatterers; eq. (5)	9
2) Rayleigh Scatterers; eq. (6)	12
3) Dominant Plus Rayleigh Scatterers; eq. (7)	12
4) Realistic Cases	16
B. Multiple Envelope Pulse Integration - N Pulses	16
1) Constant Amplitude Scatterers; eq. (8)	19
2) Rayleigh Scatterers	22
a) Slow Fluctuating Target; eq. (9)	22
b) Fast Fluctuating Target; eq. (10)	22
3) Dominant Plus Rayleigh Scatterers	29
a) Slow Fluctuating Target; eq. (11)	29
b) Fast Fluctuating Target; eq. (12)	30
4) Realistic Cases	36
VI. Conclusions	43
Appendix A - Development of the Gram-Charlier Series for Detection Probability of Constant Amplitude Scatterers	45
Appendix B - The Incomplete Toronto Function	50

I. INTRODUCTION

The equations describing radar detection probabilities of constant amplitude, Rayleigh, and dominant plus Rayleigh targets have been well known for several decades. For these scatterers, plots showing detection probability versus signal-to-noise ratio for different values of false alarm probability and number of pulses integrated have been documented by many investigators.

Woodward [1], Swerling [2], and Marcum [3], [4] introduced these basic stochastic models for radar scatterers. These early works are presented along with plotted data in an excellent treatment of the subject by DiFranco and Rubin [5]. Many ramifications pertaining to system modes and performance have been investigated. Coherent and incoherent integration and ramifications thereof have been treated in many papers [6] - [10]. These studies have contributed much understanding on such issues as fluctuation loss, collapsing loss, and diversity gain.

North [6] introduced the concepts of matched filters, effects of post-detection integration, statistical criteria for detection, optimality of a square-law detector, and fundamental significance of signal-to-noise energy ratio. Blake in [7] presents comparisons between video integration of several pulses and cumulative detection based on independent threshold crossings on successive scans. Miller and Bernstein [8] treated signal-to-noise ratio requirements for coherent integration along with detection probability where a number of parallel

filters were used to cover a given band with the overall false alarm probability held constant. Many other works on the effects of frequency diversity may be found in [9]. Recent work by Dana and Moraitis [10] included the probability of detecting a Swerling I target on two correlated observations. A second dwell was used to verify the initial detection and minimize false alarms. This technique can be applied to the radar that operates with an electronically steered beam, range-ambiguous waveforms, and frequency agility. The conditional probability of a second dwell detection given a first dwell detection (and the probability of at least one dwell detection out of two dwells) was compared with the probability of independent dwells when two separate transmission frequencies were used.

Many sequential detection approaches involving integration, either coherent or incoherent integration, have been investigated for multiple range and beam positions [11] - [13]. These approaches assumed that, at most, one target is present with some weighted probability over the sector being investigated. For example, Finn [11] conducted a study dealing with point targets on two-step and three-step sequential detection systems using different thresholds and energy levels. Preston [14] made comparisons with nonsequential performance to show improvement as a function of the number of range cells when the sequential process is optimized for multiple range cells.

Many studies have treated the over resolved effects of targets. Nitzberg [15] evaluated detection performance of a single statistic

output derived from a broadband waveform incoherently integrated over each range cell spanning the target. Also evaluated was the detection performance for incoherently integrated frequency diversity waveforms having the same bandwidth occupancy as the broadband waveform. It was shown that at the minimum signal-to-noise ratio,¹ detection performance differed by only 0.8 dB for the two approaches. Recently, Hughes [16] presented a high-resolution radar detection strategy in conjunction with a constant false alarm rate (CFAR) processor. Hughes details a comparison of single range cell detection with incoherent integrated contiguous range cell detection. Integrated range cell detection provided improved detection capability except when the target is composed of a single strong specular point.

In this paper, a detection is based on at least one threshold crossing out of the M range cells spanning the target; likewise for a false alarm when the target is absent. Sequential detection or incoherent range cell integration was not considered here. Neither were there any procedures for correlating the over resolved target signature for maximizing system output. Probability of detection as a function of signal-to-noise ratio is provided, with the number of over resolved range cells, M, as a parameter. False alarm probability for the spanned target is held constant. We shall proceed by describing our approach.

1

The signal-to-noise ratio required for a certain level of detection performance when the waveform bandwidth just resolves the individual subscatterers.

II. APPROACH

First the threshold value is determined from a selected false alarm probability. This involves the use of analytical, numerical, or graphical false alarm and threshold relationships. The various detection probability curves as a function of signal-to-noise ratio can then be plotted. Each set of curves represents the detection probability of a particular scatterer with a specified false alarm probability and resolution index, $M = 1, 2, 5$, and 10 , as a parameter. When the target occupies one range cell ($M = 1$) the target is said to be under or properly resolved. When the waveform is such that the target consists of many subscatterers ($M > 1$) the target is over resolved. M shall designate the resolution index.

The data presented in this paper shows the effects of bandwidth (or resolution) on the probability of detection where bandwidth is related to the resolution index, $M = 1, 2, 5$, and 10 . In any one set of curves, all other factors are held constant over the different M values, i.e. false alarm probability for the entire target, total energy backscattered, and the number of pulses.

The range dependent average cross section is assumed to be uniformly distributed for all scatterers. Although this may seem to be a special case, it does lead to an upper bound in performance (the most optimum detection probabilities) for increasing M . Scatterers arbitrarily distributed over their M range cells yield less optimistic detection probabilities for increasing M . Such behavior is expected due

to the introduction of collapsing noise into the receiver. Collapsing noise is created when some of the received data samples have lower signal-to-noise ratio than that of other received data samples.²

III. FALSE ALARM AND THRESHOLD DETERMINATION

In establishing radar detection criteria it is necessary to first determine an allowable false alarm probability, P_{fa} . From this value one can determine a threshold setting for the receiver output. A false alarm occurs when the target is absent and the noise at the receiver output exceeds the threshold. If the target is over resolved, i.e. $M > 1$, then a false alarm occurs when the noise from at least one of the M over resolved range cells exceeds the threshold. Mathematically the probability of such a false alarm for the single pulse case is written

$$P_{fa} = 1 - [1 - \exp(- Y_b)]^M \quad (1).$$

where Y_b denotes the threshold to noise energy setting per cell. The expression for the multiple pulse case of N incoherent integrated pulses is written

2

See reference [17] for a discussion on collapsing noise.

$$P_{fa} = 1 - \left[I\left(\frac{Y_b}{\sqrt{N}}, N-1 \right) \right]^M \quad (2).$$

$I(.,.)$ is the incomplete gamma function. In the above equations the threshold setting will be dependent on P_{fa} , the false alarm probability, M , the number of range cells into which the target has been over resolved, and N , the number of pulses.

Analytical, numerical, and graphical solutions (in that order whichever the case may be) were used to determine the receiver threshold. Threshold values were determined for each of the given values of false alarm probability, resolution index, M , and number, N , of incoherent integrated pulses per cell.

IV. DECISION RULE FOR SCATTERER DETECTION

A detection is declared whenever at least one threshold crossing occurs out of the M subscatterer range cells spanning the target. The example in figure 1 illustrates this point. For scatterer A, only one threshold crossing out of five subscatterers investigated is observed and so scatterer A is detected. For scatterer B, three threshold crossings are observed, thus scatterer B is also detected. Each subscatterer response in figure 1 represents a N pulse integrated variable where $N \geq 1$. The receiver for such a decision rule is shown in figure 2.

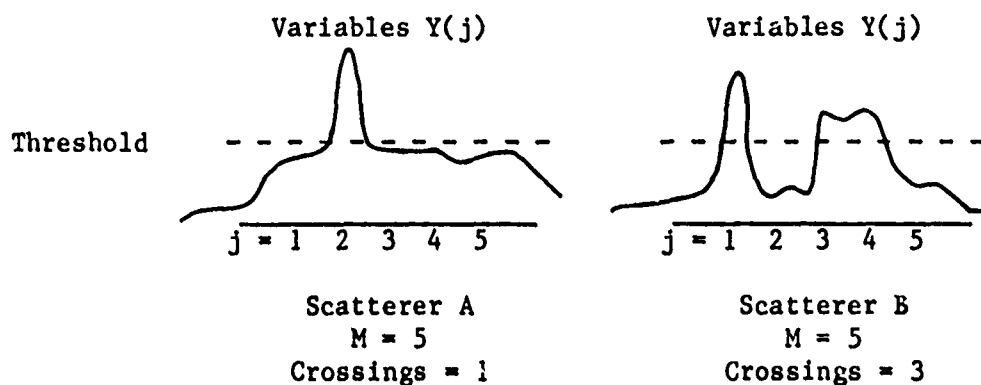


Figure 1. Example of the Threshold Crossings for $M = 5$ Subscatterers.

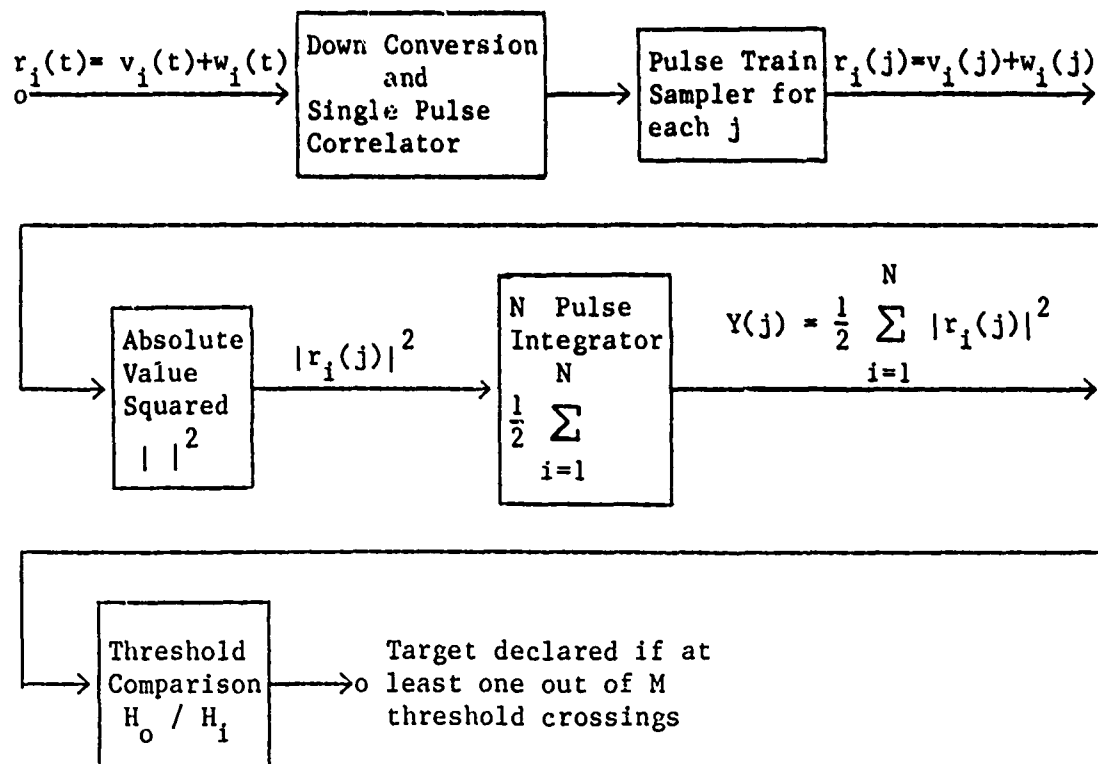


Figure 2. Receiver Structure for Detecting an Incoherent Pulse Train.

The index, j ($j = k+1, k+2, \dots, k+M$ for any k), denotes the j th range cell while the index, i ($i = 1, 2, 3, \dots, N$), denotes the i th pulse. A target is declared when at least one $Y(j)$ exceeds the predetermined threshold Y_b , i.e.

$$\begin{aligned} \bigcup_{j=1}^M Y(j) > Y_b & : H_1 \text{ Target declared} \\ \bigcap_{j=1}^M Y(j) \leq Y_b & : H_0 \text{ Target not declared} \end{aligned}$$

If the probability of a single threshold crossing out of M subscatterer cells is P_{DM} , then from the binomial formula the probability P_D of at least one crossing out of M cells is

$$P_D = 1 - (1 - P_{DM})^M \quad (3).$$

The computation of P_{DM} depends on the scatterer model, waveform, bandwidth (resolution index), threshold setting, signal-to-noise ratio, and the number of pulses being considered. In the following sections we provide the expression for P_{DM} under such conditions. Expressions for the subscatterer probability of detection, P_{DM} , are obtained from [5] with appropriate modifications on signal energy, \bar{E} . The total average energy backscattered from all the subscatterers will be held constant. This is written as follows

$$\bar{E} = \sum_{i=1}^M \bar{E}_M = M \bar{E}_M \quad (4).$$

where \bar{E} denotes the average energy backscattered from the entire scatterer and \bar{E}_M denotes the average energy backscattered from each of the M subscatterers. Since the energy distribution backscattered across the scatterer is assumed uniformly distributed, the relationship $\bar{E}_M = \bar{E}/M$ holds.

V. DETECTION PROBABILITY - TARGET OF M RANGE CELLS

A. SINGLE PULSE WAVEFORM (N = 1)

First we consider a waveform consisting of one single pulse. Three target models are evaluated having the following subscatterers.

- 1) Constant amplitude scatterers
- 2) Rayleigh scatterers
- 3) Dominant plus Rayleigh scatterers

In the following discussion, the probability of detection is plotted as a function of the signal-to-noise ratio energy per pulse backscattered from the target.

1) Constant Amplitude Scatterers

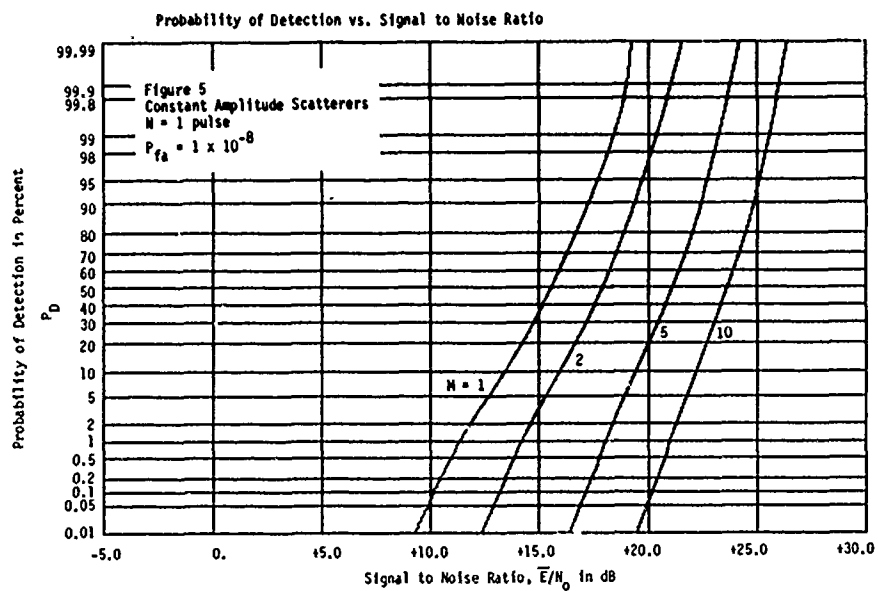
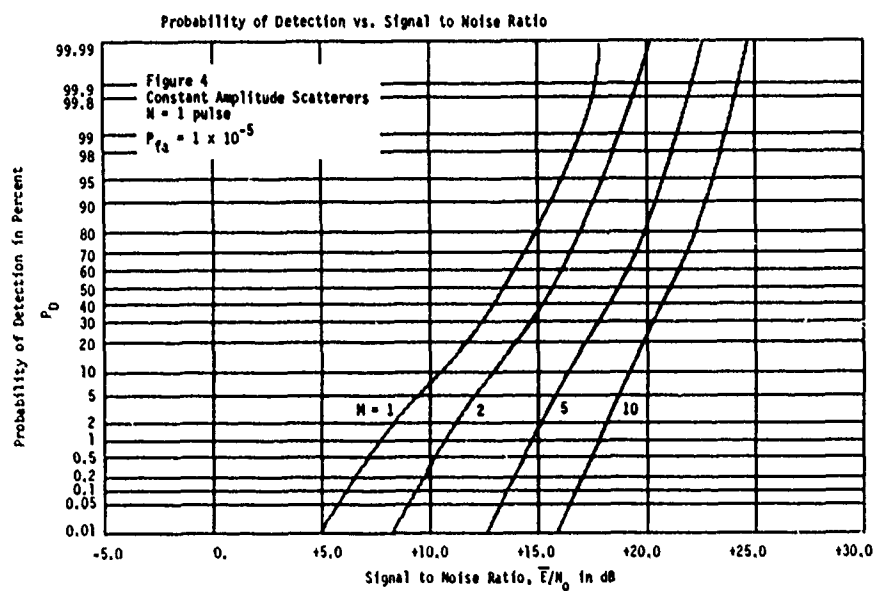
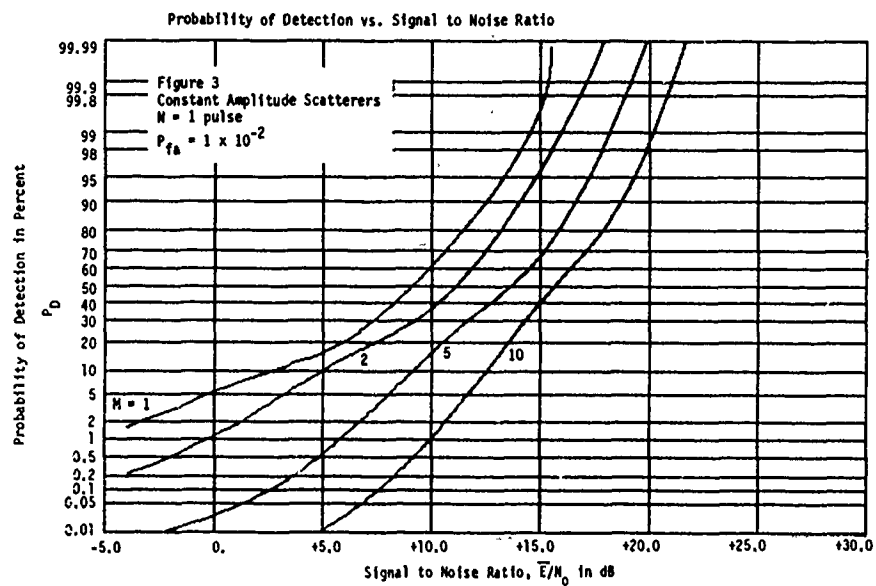
A scatterer which has a nonrandom amplitude and a uniformly distributed phase is denoted a constant amplitude scatterer. For

constant amplitude scatterers, the detection probability, P_D , for at least one hit out of M hits, each hit having a detection probability of P_{DM} , is given by equation (3) where

$$P_{DM} = 1 - T_{\sqrt{Y_b}}[1, 0, \sqrt{\bar{E}/MN_o}] \quad (5).$$

\bar{E}/M is the average energy in the received signal from each subscatterer and $T_y[i, j, k]$ is the incomplete Toronto function [3], [4], [18] - [20] with threshold to noise energy ratio, y^2 , and arguments i , j , and k . For the constant amplitude case, $\bar{E} = E$. A four term expansion of the incomplete Toronto function is carried out in appendix A. Appendix B provides a discussion on how the incomplete Toronto function relates to probability theory.

For constant amplitude subscatterers, the probability of detection as a function of the signal-to-noise ratio is shown in figures 3, 4, and 5. For each value of M , the constant amplitude scatterer model has been reconfigured into M constant amplitude subscatterers each randomly located within each of the M range cells. Thus, each of the curves in these figures represents a different structure, e.g. one sphere for $M = 1$, two spheres for $M = 2$, etc. The only common characteristics are false alarm probability, P_{fa} , and total signal energy, \bar{E} . The detection probability degrades as the resolution index, M , increases for all values of signal-to-noise ratio. This results in an apparent signal-to-noise ratio loss.



2) Rayleigh Scatterers

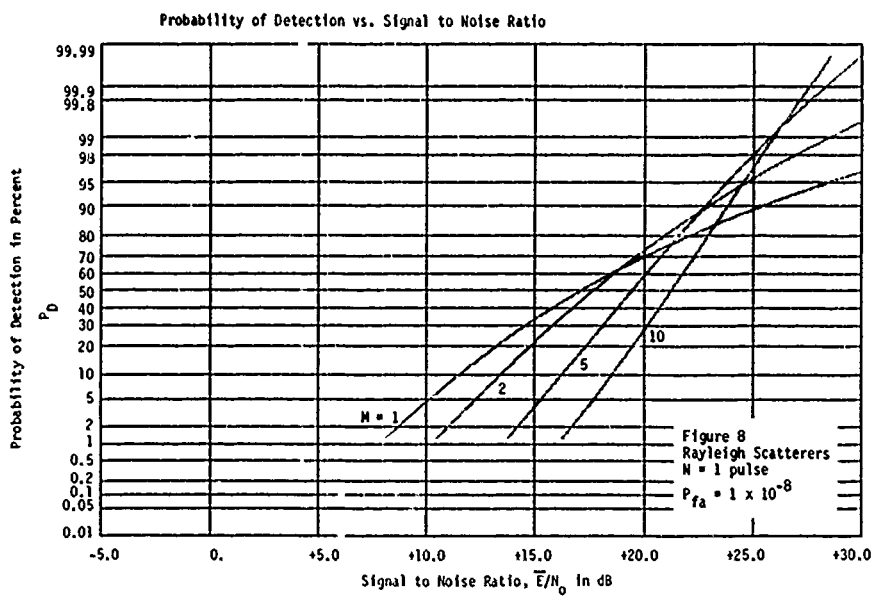
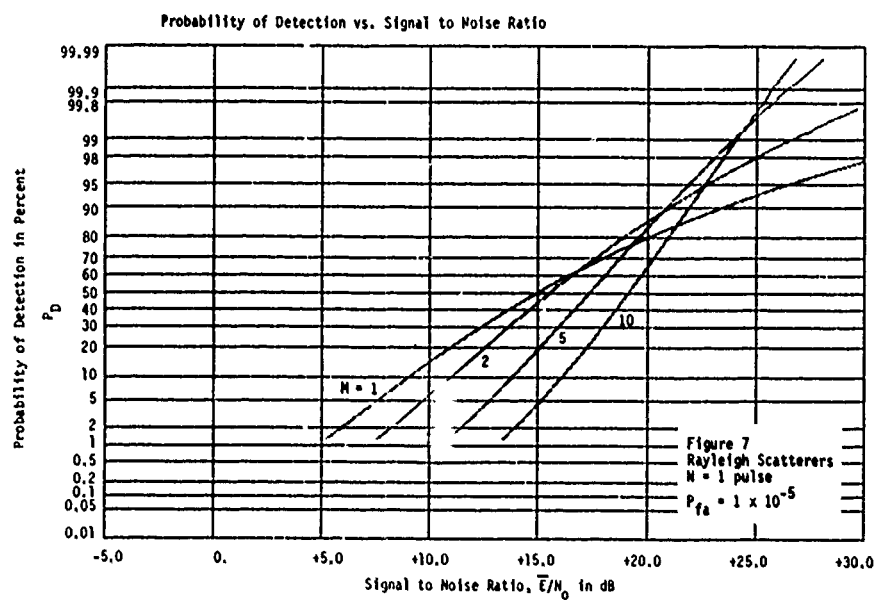
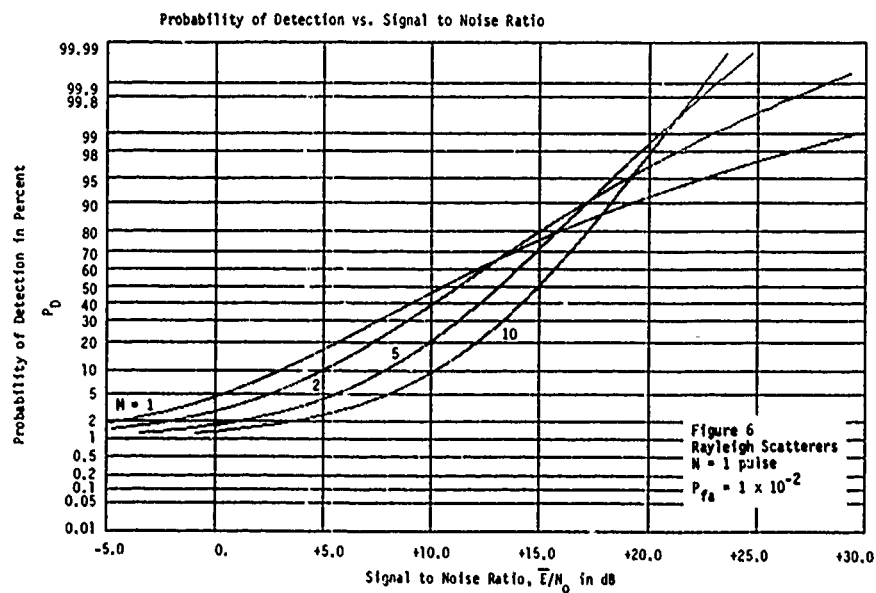
For Rayleigh subscatterers, the detection probability, P_D , for at least one hit out of M possible hits, each hit having a detection probability of P_{DM} , is given by equation (3) where

$$P_{DM} = \exp\left[- \frac{Y_b}{(1 + \bar{E}/2MN_0)} \right] \quad (6).$$

For Rayleigh subscatterers the probability of detection as a function of the signal-to-noise ratio is shown in figures 6, 7, and 8. Since for each value of M the scatterer model is complex Gaussian (Rayleigh), then each of the curves in these figures may represent the same scatterer by virtue of the property: the superposition of Gaussian random variables results in a Gaussian random variable. It can be seen that an improvement in detection probability results as the resolution index, M , increases for larger values of signal-to-noise ratio. An increased resolution index, M , results in an increase in gain for larger values of signal-to-noise ratio but results in a loss for the lower signal-to-noise ratios.

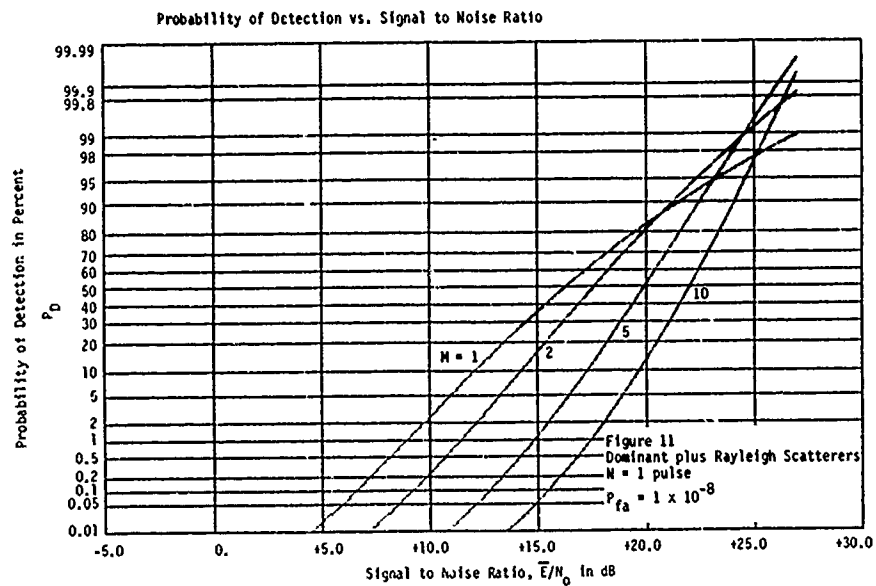
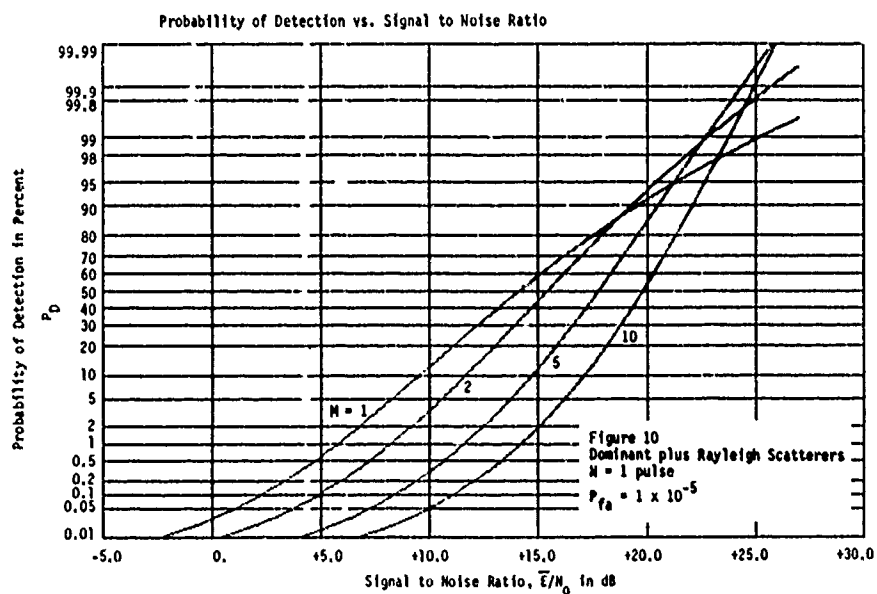
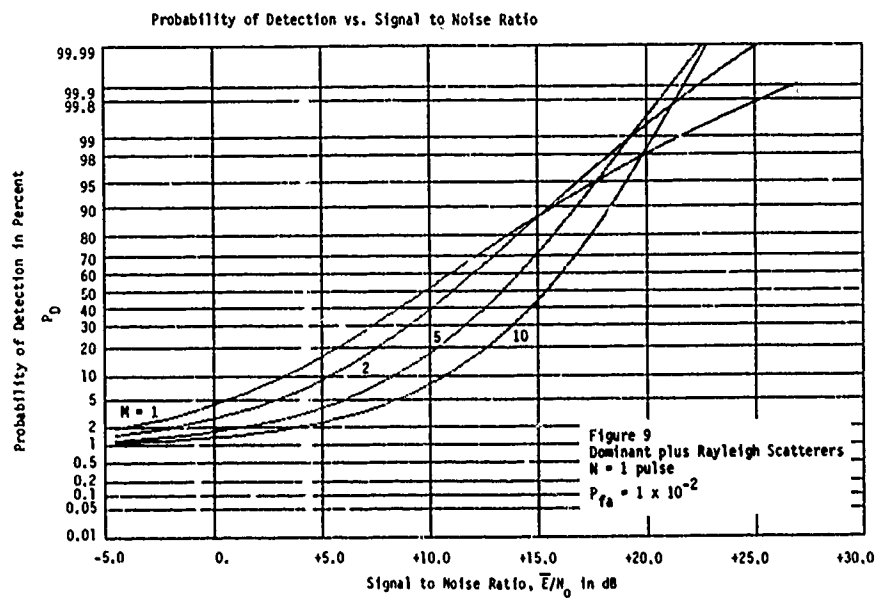
3) Dominant Plus Rayleigh Scatterers

For the dominant plus Rayleigh subscatterers, the detection probability, P_D , for at least one hit out of M possible hits, each hit having a detection probability of P_{DM} , is given by equation (3) where



$$P_{DM} = \left(\frac{1}{1 + 4MN_0/\bar{E}} \right) \left(1 + \frac{4MN_0}{\bar{E}} + \frac{Y_b}{1 + \bar{E}/4MN_0} \right) \exp \left(- \frac{Y_b}{1 + \bar{E}/4MN_0} \right) \quad (7).$$

For dominant plus Rayleigh subscatterers the probability of detection as a function of the signal-to-noise ratio is shown in figures 9, 10, and 11. Again the scatterer has been reconfigured into M dominant plus Rayleigh subscatterers each randomly located within each of the M range cells. M dominant plus Rayleigh subscatterers do not quite superimpose to result in a M = 1 dominant plus Rayleigh target. Instead a Rayleigh target would result. These curves, however, do represent the same overall false alarm probability, P_{fa} , and total signal energy, \bar{E} , over the length of the target. The appropriate comparisons are discussed in the next paragraph. In these figures there is an apparent slight improvement in detection probability as the resolution index, M, increases for larger values of signal-to-noise ratio. For lower false alarm probabilities a larger signal-to-noise ratio, \bar{E}/N_0 , is required in order to maintain the same detection probability. This scatterer represents a case where the dominant part of the scatterer acts as the constant amplitude scatterer of 1) above and the "plus Rayleigh" part acts as the Rayleigh scatterer of 2) above.

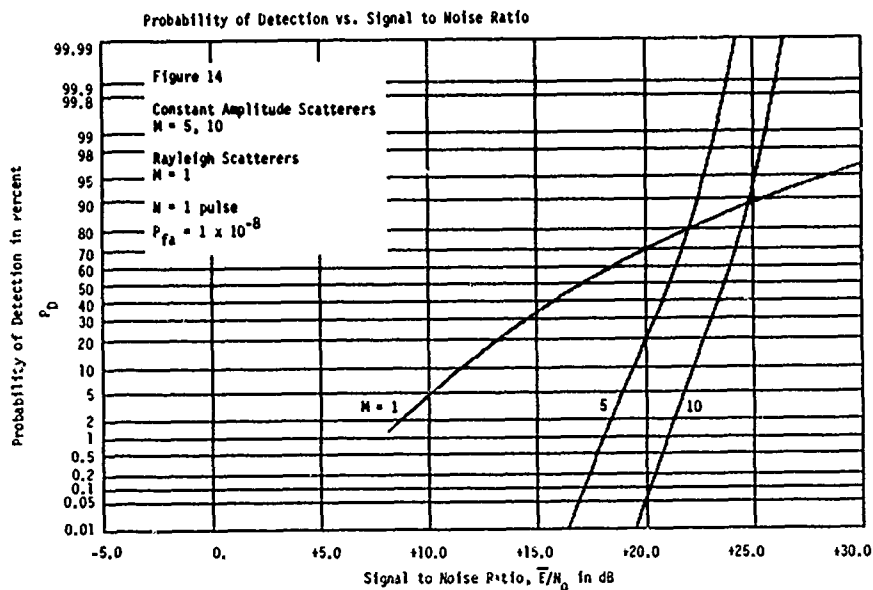
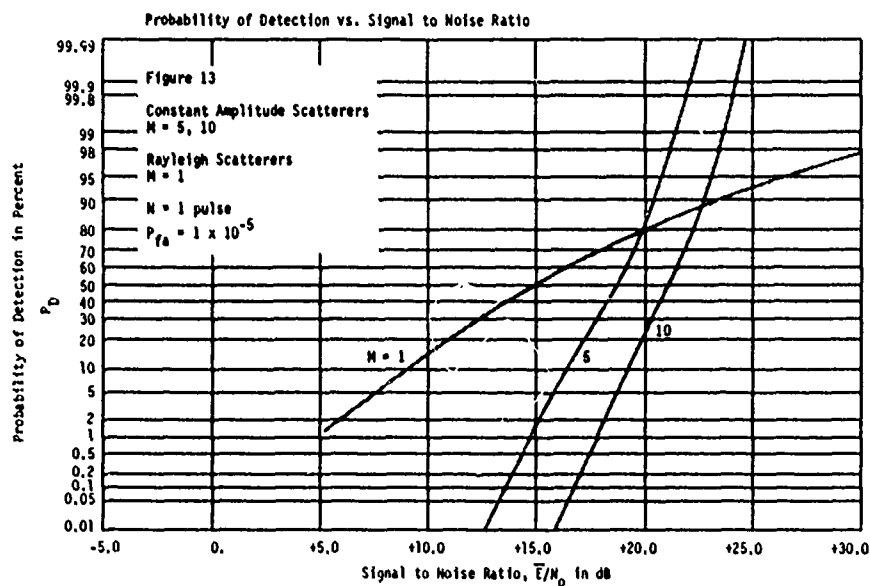
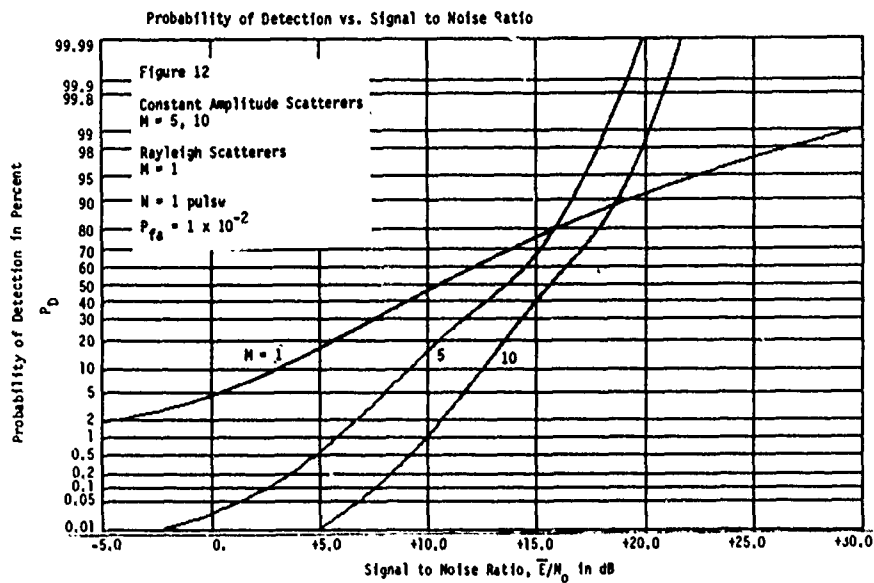


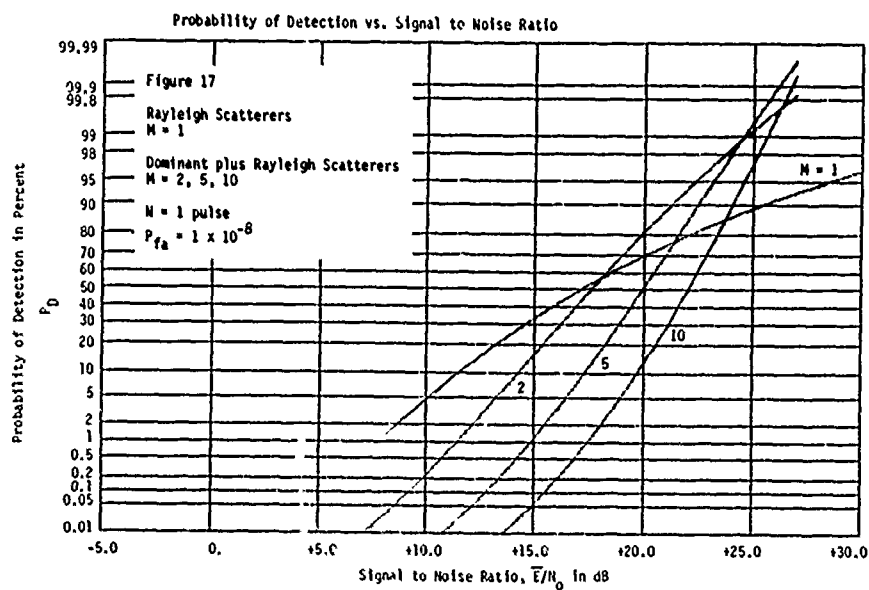
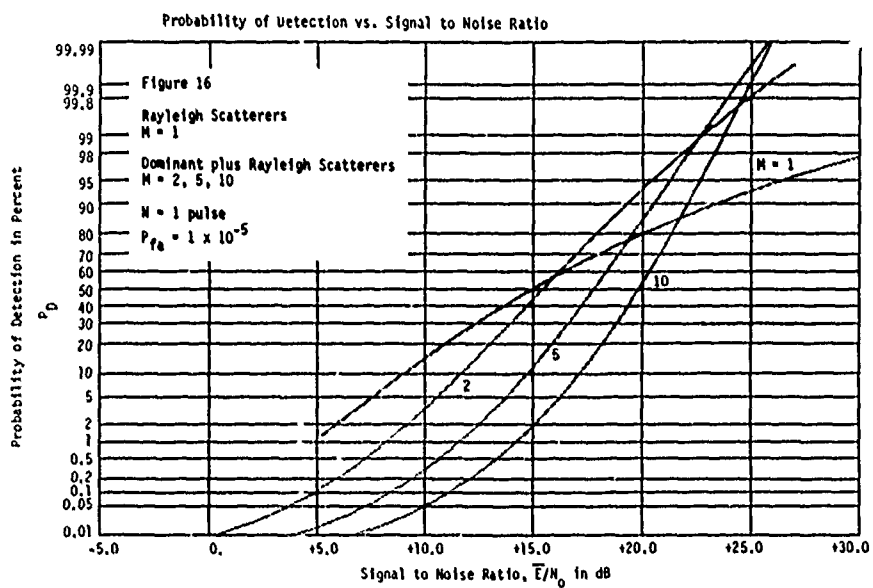
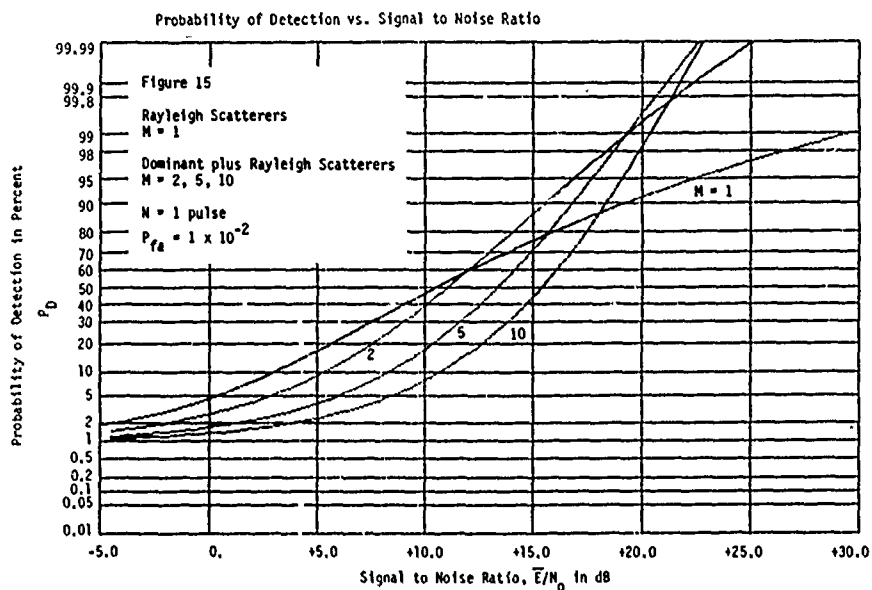
4) Realistic Cases

In reality, a scatterer consisting of equal amplitude and/or dominant plus Rayleigh subscatterers approaches a complex Gaussian (Rayleigh) scatterer as the number of subscatterers increases. This is validated by virtue of the central limit theorem and holds for all the subscatterer models considered above. To evaluate these realistic cases we plot the detection probability of the Rayleigh scatterer for $M = 1$ with the detection probability of its constituent constant amplitude subscatterers for $M = 5$ and 10 . The result is shown in figures 12, 13, and 14. It can be seen that for resolution indices of around $M = 5$, a marked improvement in performance occurs as the signal-to-noise ratios increase beyond that corresponding to 80% detection probability. It should be kept in mind that correspondingly, a loss occurs below the 80% probability, i.e. at low signal-to-noise ratios. Similar improvements for the Rayleigh scatterer consisting of dominant plus Rayleigh subscatterers are illustrated in figures 15, 16, and 17.

B. MULTIPLE ENVELOPE PULSE INTEGRATION - N PULSES

We now consider waveforms consisting of a train of N pulses and the scatterer divided into M subscatterers. The same subscatterers treated previously will be considered with the addition of their fluctuation characteristics.





- 1) Constant amplitude scatterers
- 2) Rayleigh scatterers
 - a) Slow fluctuating target
 - b) Fast fluctuating target
- 3) Dominant plus Rayleigh scatterers
 - a) Slow fluctuating target
 - b) Fast fluctuating target

In the probability of detection plots which follow, the independent variable is signal-to-noise ratio energy per pulse backscattered from the target.

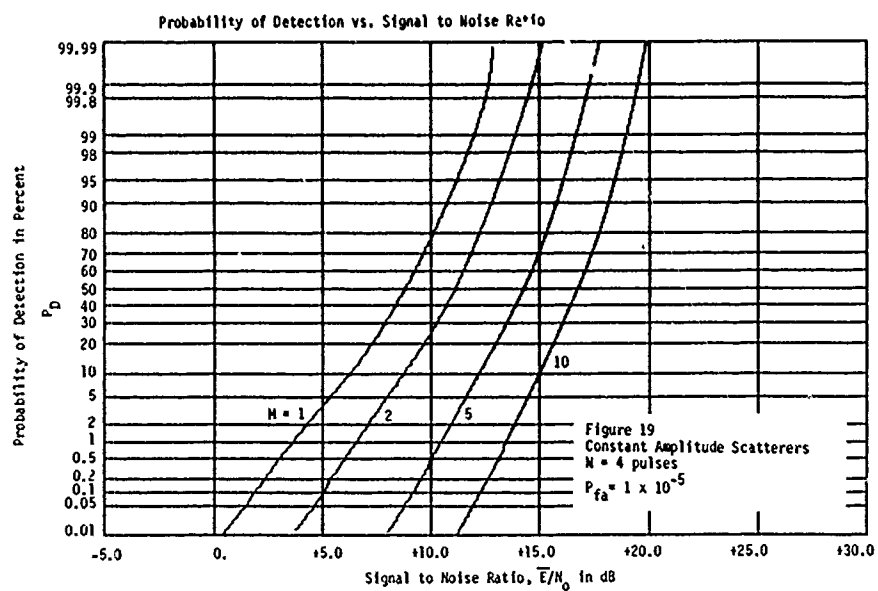
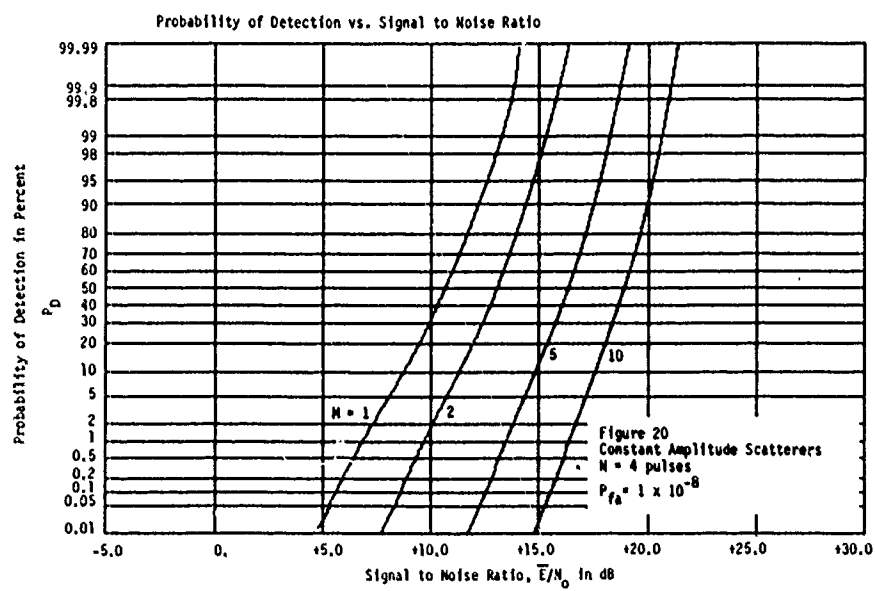
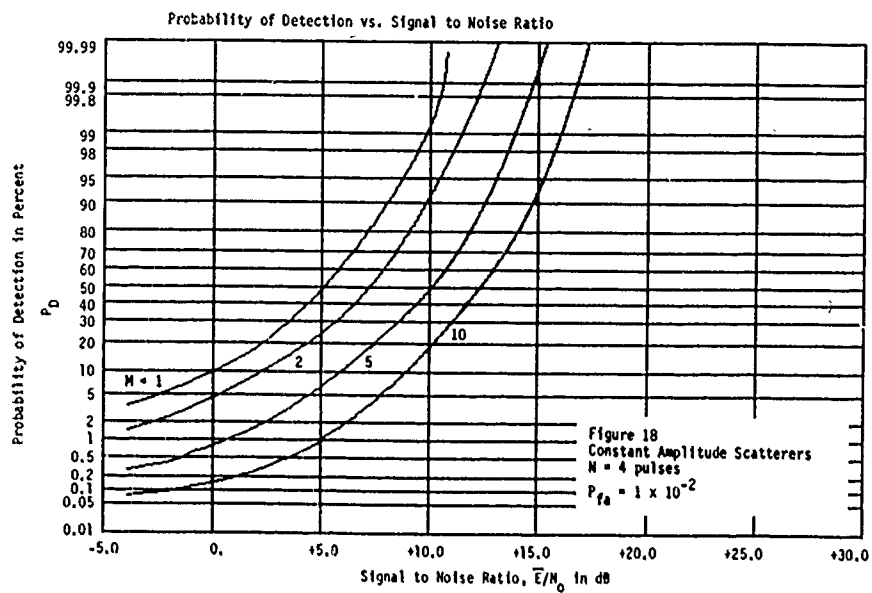
1) Constant Amplitude Scatterers

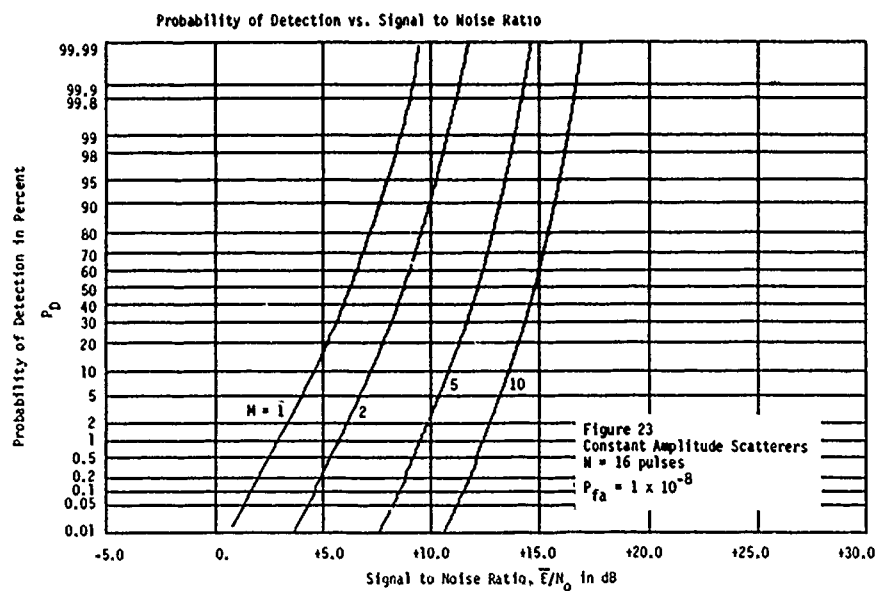
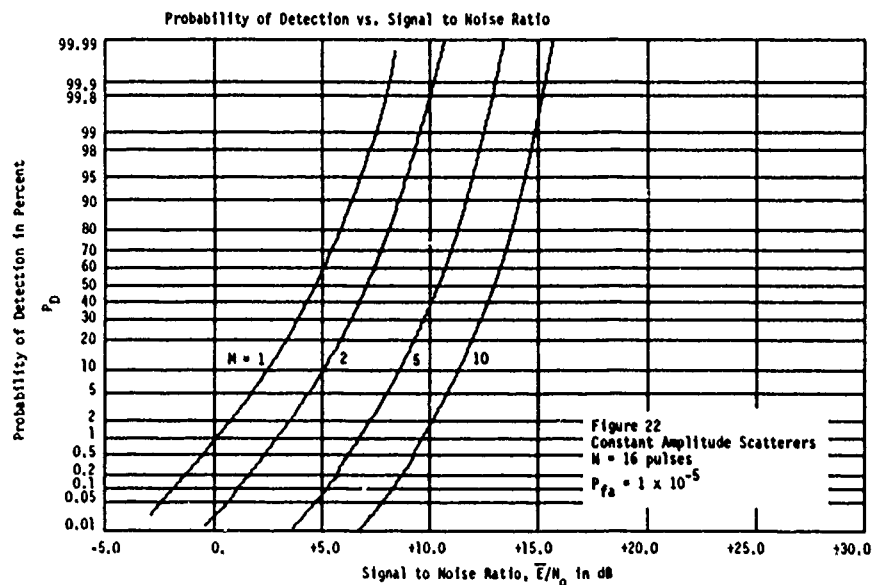
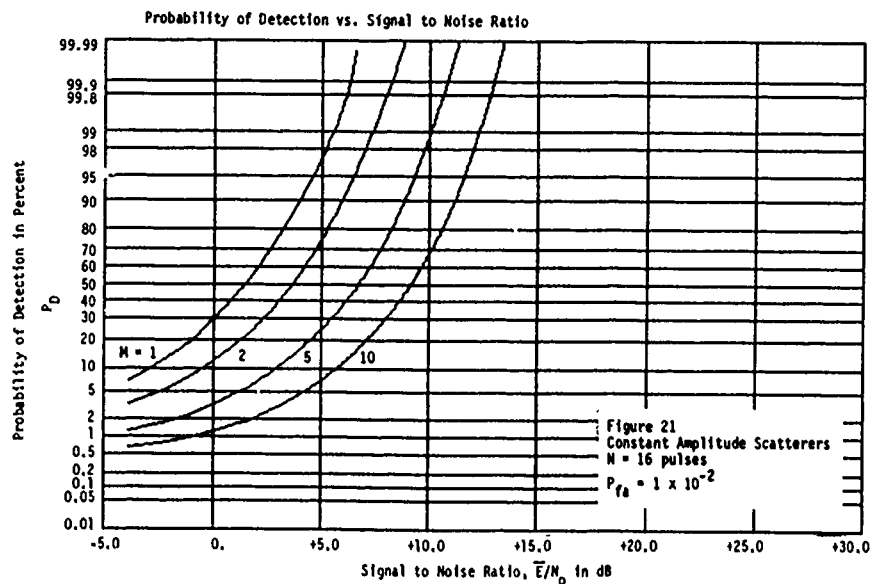
The detection probability for the constant subscatterers is given by equation (3) where

$$P_{DM} = 1 - T_{\sqrt{Y_b}} [2N-1, N-1, \sqrt{NE/MN_0}] \quad (8).$$

For the constant amplitude case, $\bar{E} = E$.

For the constant amplitude target, the probability of detection as a function of the signal-to-noise ratio is shown in figures 18, 19, and 20 for a four pulse train, $N = 4$, and in figures 21, 22, and 23 for $N = 16$. Again, as in figures 3, 4, and 5, for each value of M , the constant amplitude scatterer model has been reconfigured into M constant amplitude subscatterers each randomly located within each of the M range cells. Thus, each of the curves in these figures represents a different





scatterer where the only common characteristics are false alarm probability, P_{fa} , total signal energy, \bar{E} , and the number of pulses, N . The best performance is achieved for a resolution index of $M = 1$. Detection probability decreases for any signal-to-noise ratio as the resolution index, M , increases.

2) Rayleigh Scatterers

For M Rayleigh subscatterers the detection probability is given by equation (3) where

a) for a slow fluctuating target

$$P_{DM} = 1 - I\left[\frac{Y_b}{\sqrt{N-1}}, N-2\right] + \left[1 + \frac{1}{N\bar{E}/2MN_0}\right]^{N-1} \times \exp\left[-\frac{Y_b}{1 + N\bar{E}/2MN_0}\right] \times I\left[\frac{Y_b}{\sqrt{N-1} (1 + 2MN_0/N\bar{E})}, N-2\right] \quad (9)$$

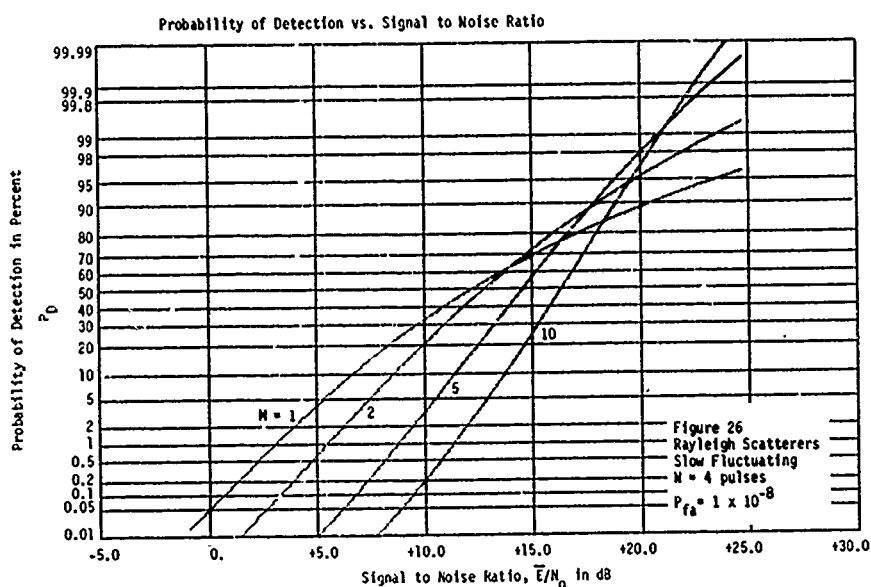
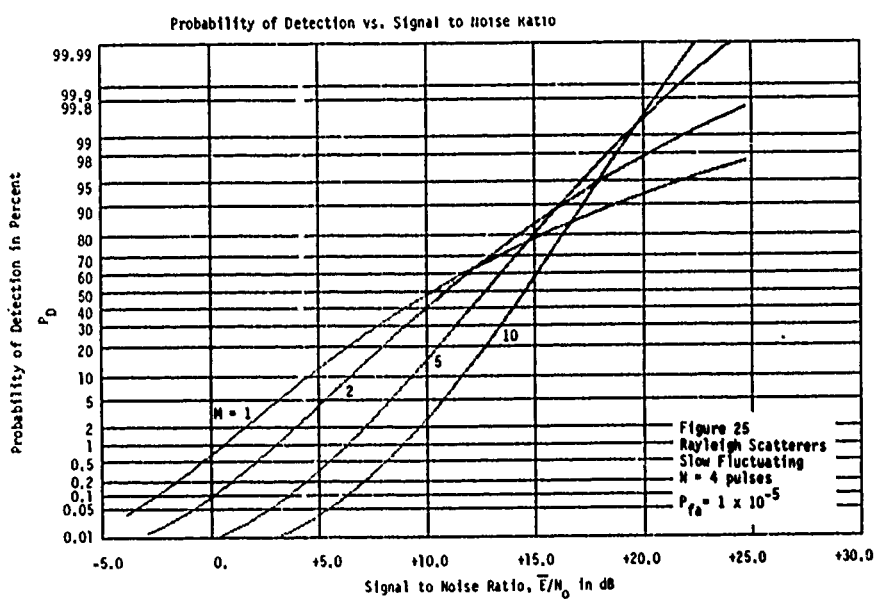
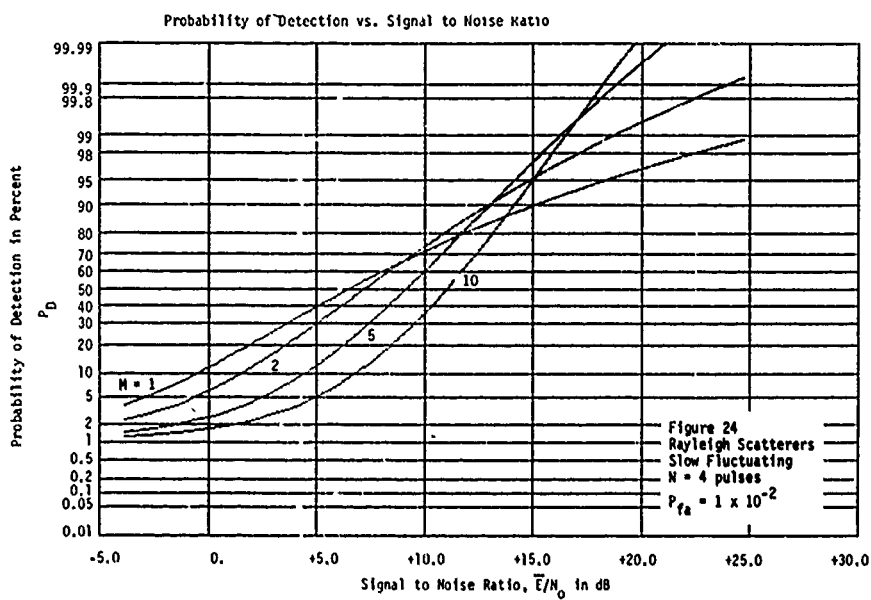
b) and for a fast fluctuating target

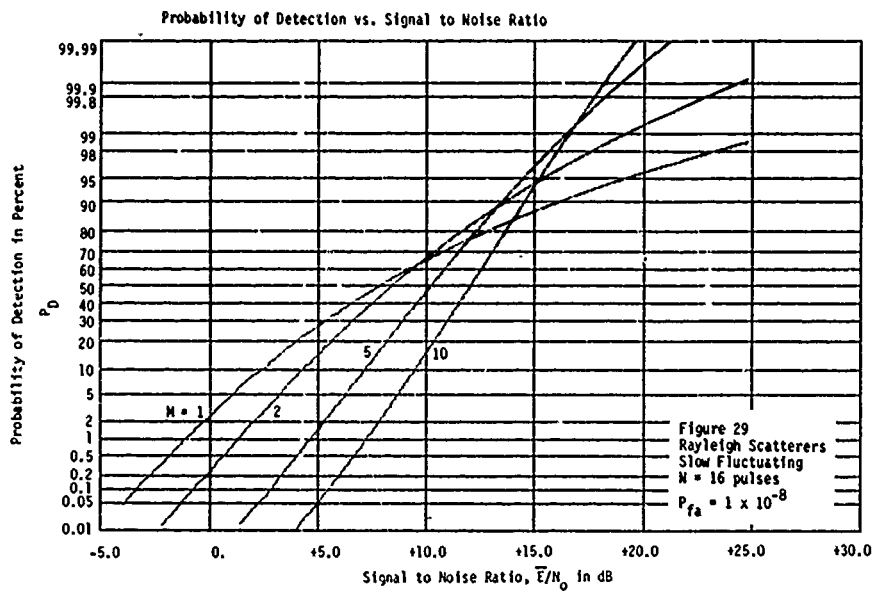
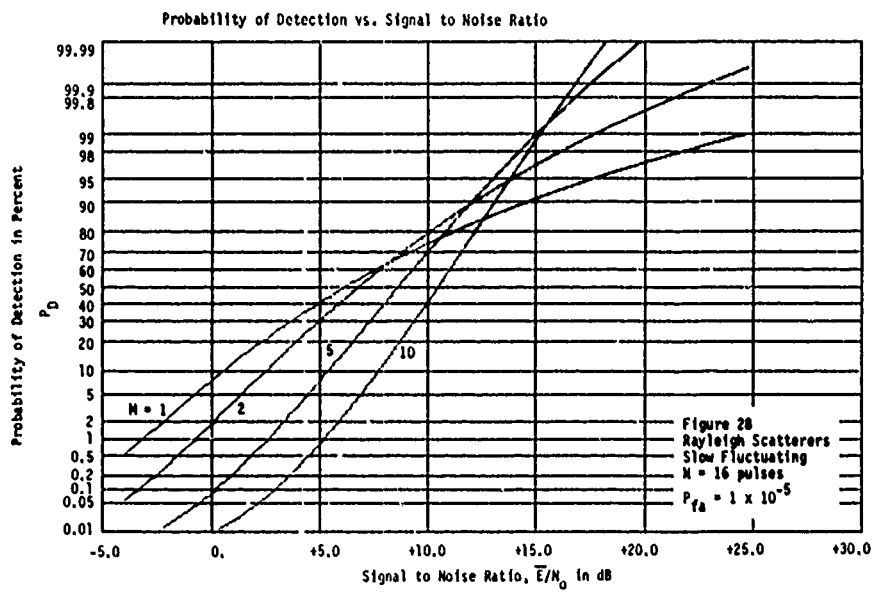
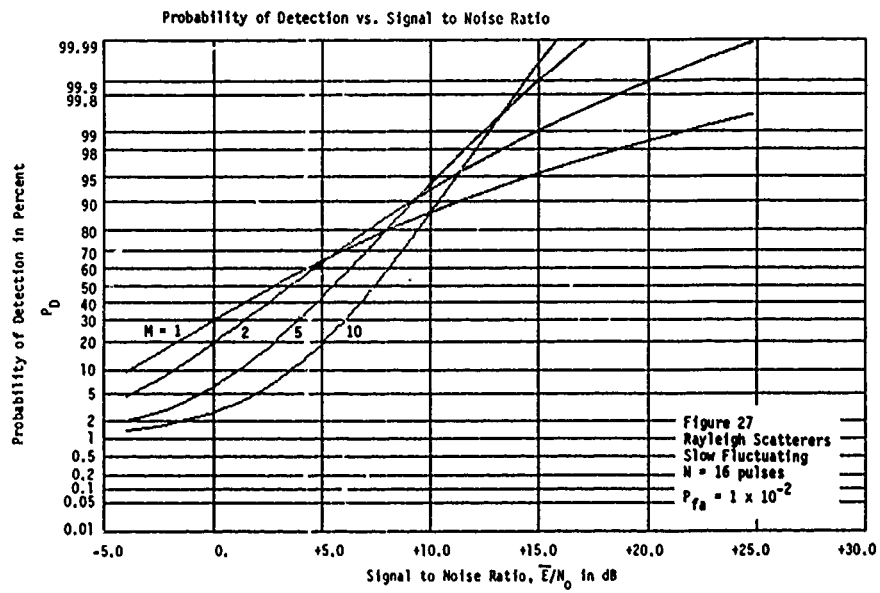
$$P_{DM} = 1 - I\left[\frac{Y_b}{\sqrt{N} (1 + \bar{E}/2MN_0)}, N-1\right] \quad (10).$$

$I[.,.]$ is the incomplete gamma function.

For the Rayleigh slow fluctuating target the probability of detection as a function of the signal-to-noise ratio is shown in figures 24, 25, and 26 for $N = 4$ and in figures 27, 28, and 29 for $N = 16$. As discussed after equation (6), each of the curves in each figure represents detection performance derived from the same scatterer. Such a relationship is a consequence of the fact that the sum of Gaussians is a Gaussian. Note that in figure 24 the detection probability increases at a larger rate with respect to signal-to-noise ratio for increasingly higher values of M . In figure 24 for $M = 2$, there is improved detection performance with respect to $M = 1$ when the signal-to-noise ratio exceeds 8.9 dB. For signal-to-noise ratios above 13.1 dB, maximum performance is obtained for a resolution index of $M = 5$. Above 17.1 dB maximum performance is obtained for a resolution index of $M = 10$. Similar effects are noted in figures 25 through 29. For lower false alarm probabilities these crossover points occur at a higher signal-to-noise ratio. On the other hand, detection probability deteriorates for increasingly higher values of M when the signal-to-noise ratio is low.

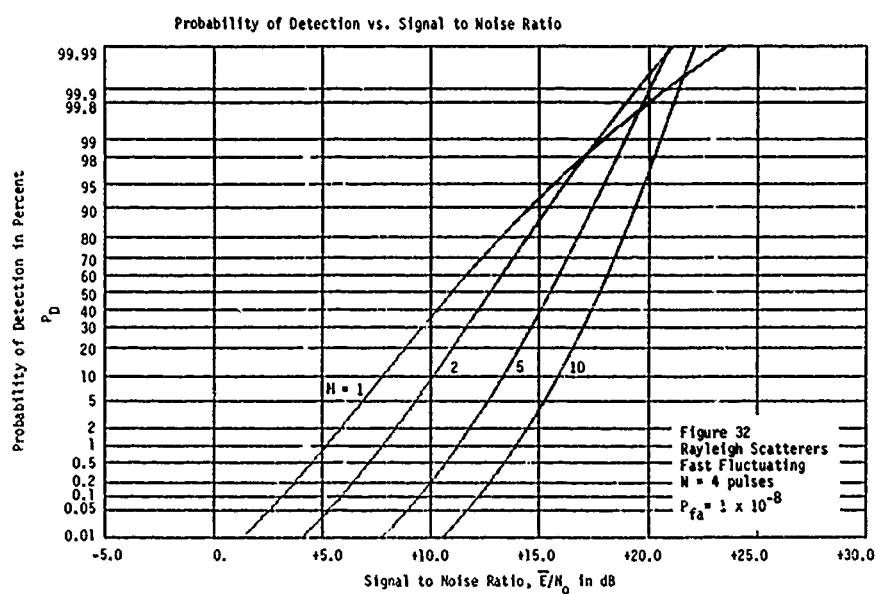
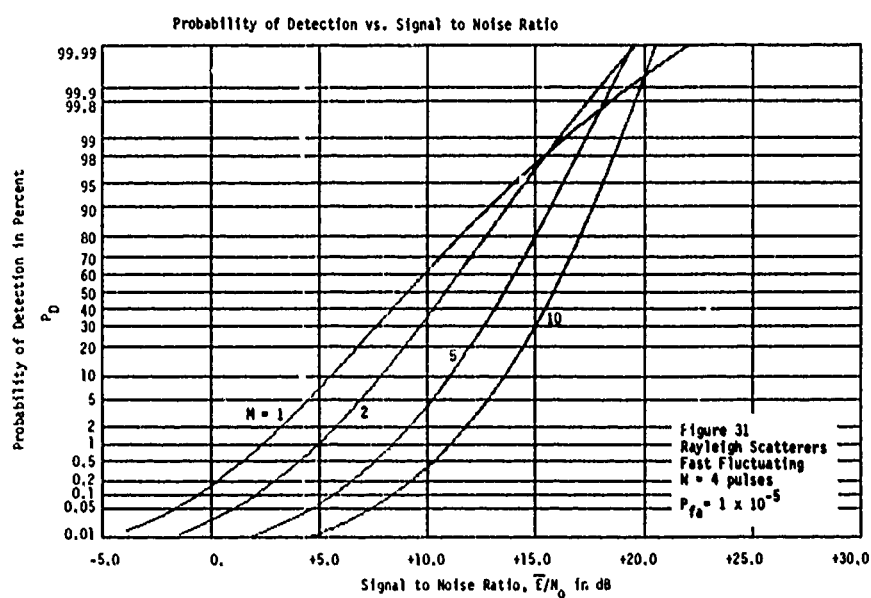
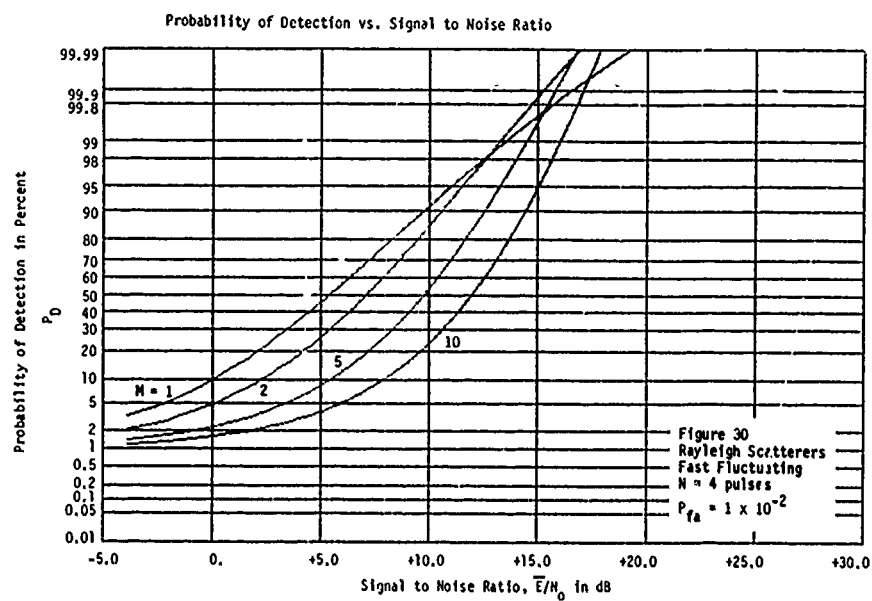
For the Rayleigh slow fluctuating target, the N pulse samples from each subscatterer are dependent; therefore, the scatterer amplitude estimate at the output of the integrator has the same proportionate variance as that of the single pulse case for all M . Its detection performance has a similar relationship with respect to M as that of the Rayleigh target single pulse case. Compare figures 24 through 29 with figures 6 through 8.

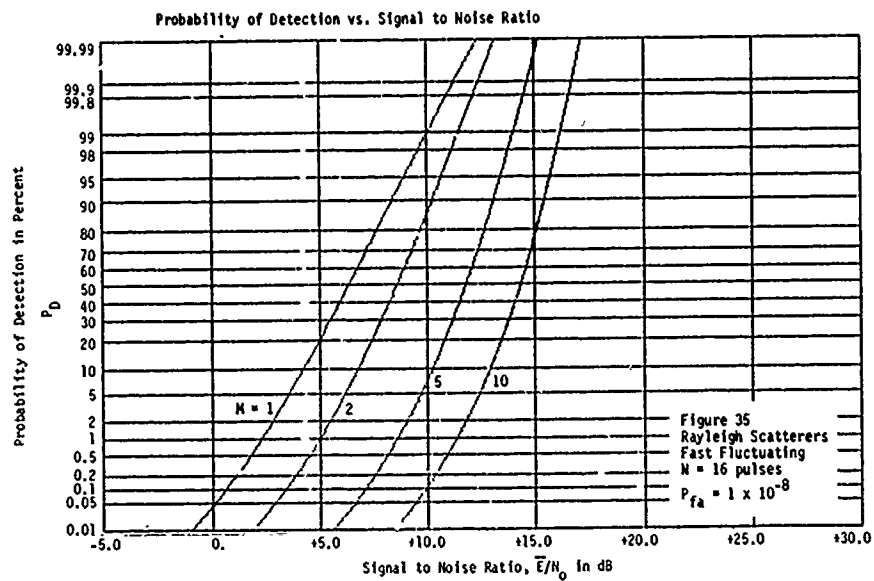
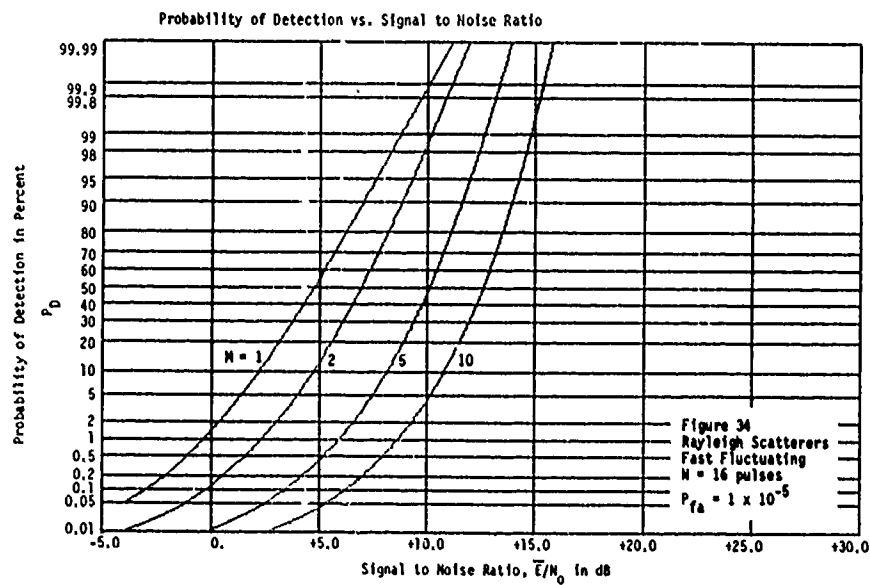
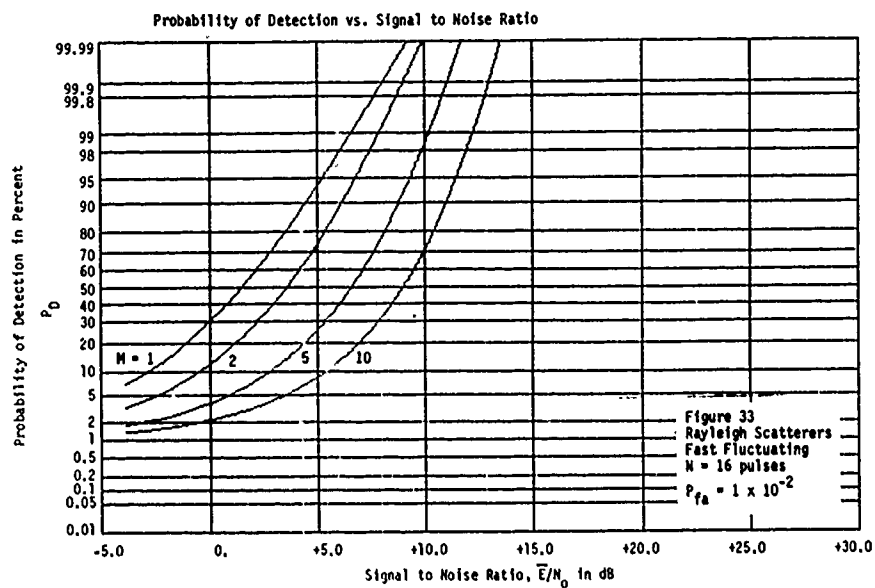




For the Rayleigh fast fluctuating target the probability of detection as a function of the signal-to-noise ratio is shown in figures 30, 31, and 32 for $N = 4$ and in figures 33, 34, and 35 for $N = 16$. Here, the amplitude of each of the M subscatterers has been estimated by inputting N independent samples into the N pulse integrator shown in figure 2. As N increases the estimate, $Y(j)$, approaches that of the M constant amplitude subscatterers. Under these conditions, the curves for each M represent the same target. As the number of pulses, N , increases, the detection probability tends to degrade for all values of signal-to-noise ratio for increasingly higher values of M as was the case for the constant amplitude scatterers of figures 18 through 23.

Note, the improvement that was derived from increasing M in the Rayleigh single pulse case or the Rayleigh slow fluctuating target case does not occur with increasing N in the fast fluctuating target case. For example, in the fast fluctuating scatterer of figure 30, the $M = 2$ case outperforms the $M = 1$ case when the signal-to-noise ratio exceeds 12.7 dB. From figure 24, i.e. the Rayleigh slow fluctuating scatterer, the crossover point was at 8.9 dB. As the number of independent samples, N , increases as in figure 33 through 35, the estimated amplitude approaches that of the constant amplitude case, i.e. the error variance decreases. Also, the detection performance approaches that of the constant amplitude case. Comparing figures 30 through 35 with figures 18 through 23 a striking resemblance is observed between the N pulse fast fluctuating target and the constant amplitude target.





3) Dominant Plus Rayleigh Scatterers

For M dominant plus Rayleigh subscatterers the detection probability is given by equation (3) where

a) for a slow fluctuating target

$$P_{DM} = \int_{Y=Y_b}^{Y=\infty} p(Y) dY \quad (11).$$

$p(Y)$ is given below. This integral is evaluated using numerical integration.

$$p(Y) = \frac{\left[1 + \frac{1}{N\bar{E}/4MN_o} \right]^{N-2}}{(1 + N\bar{E}/4MN_o)^2} > Y > K > \exp\left(- \frac{Y}{1+N\bar{E}/4MN_o} \right) +$$

$$- \frac{(N-2) \left[1 + \frac{1}{N\bar{E}/4MN_o} \right]^{N-1}}{(1 + N\bar{E}/4MN_o)^2} > K > \exp\left(- \frac{Y}{1+N\bar{E}/4MN_o} \right) +$$

$$\frac{Y^{N-1} \exp(-Y)}{(N-2)! (1 + N\bar{E}/4MN_o)^2}$$

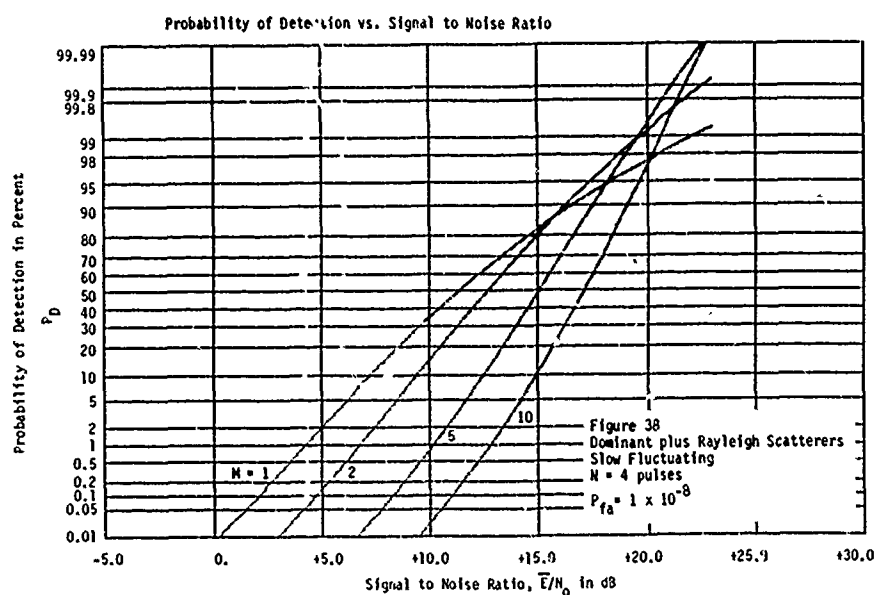
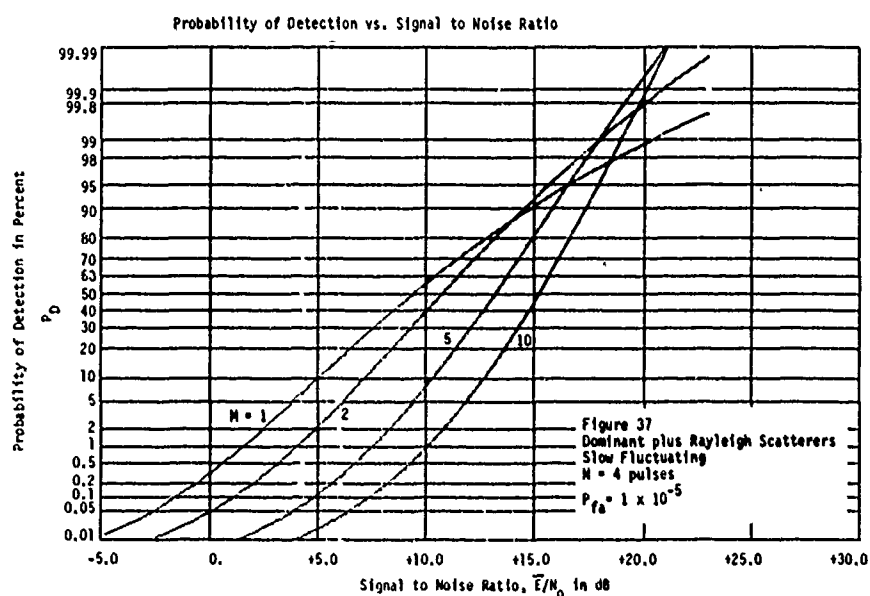
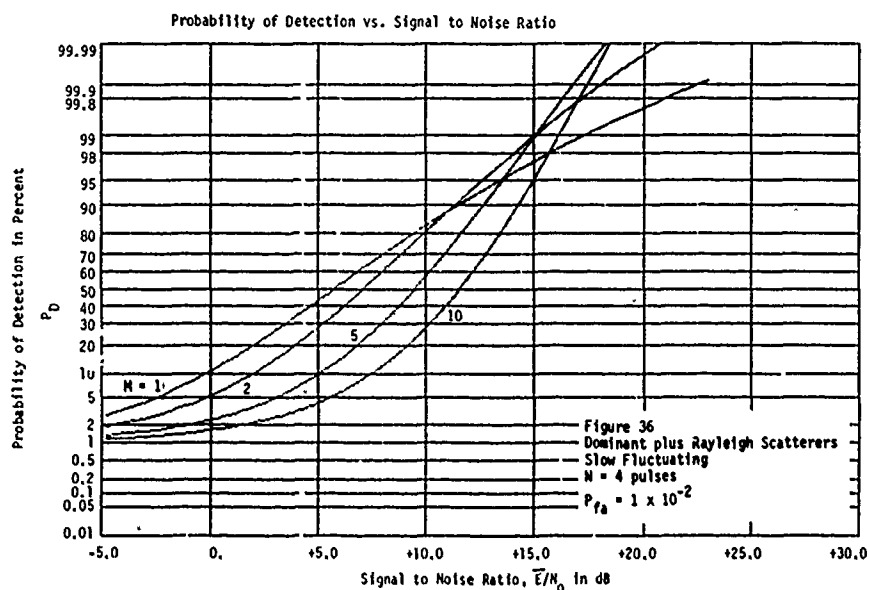
where $K = I \left[\frac{Y}{\left(1 + \frac{1}{N\bar{E}/4MN_0} \right) \sqrt{N-1}}, N-2 \right]$

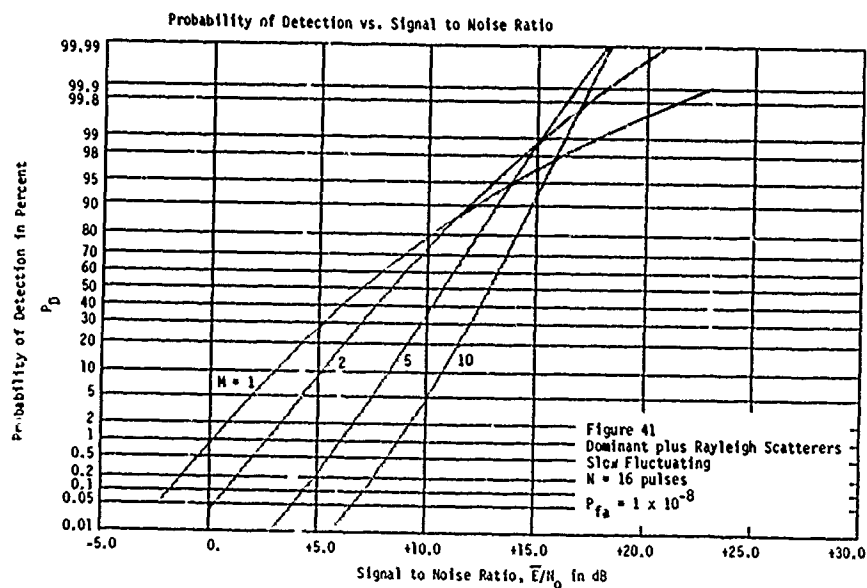
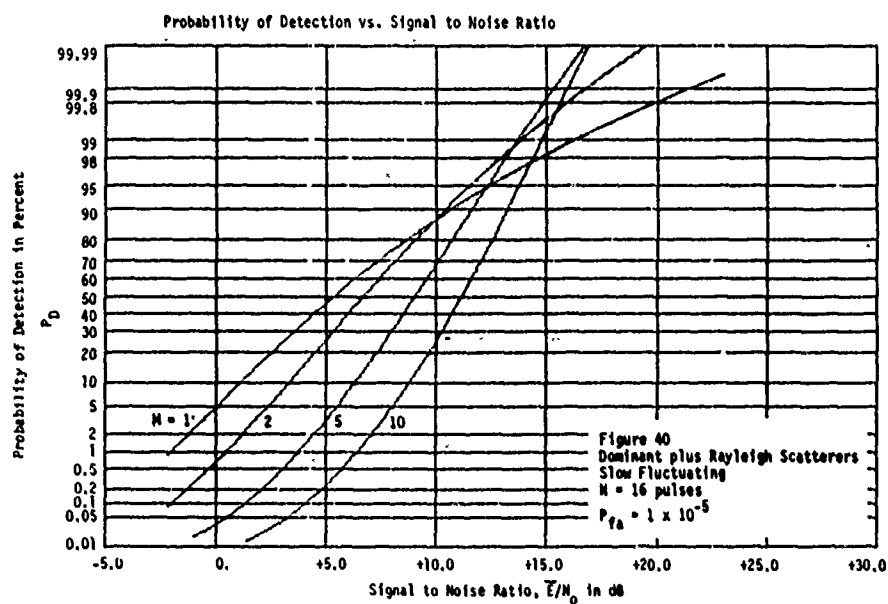
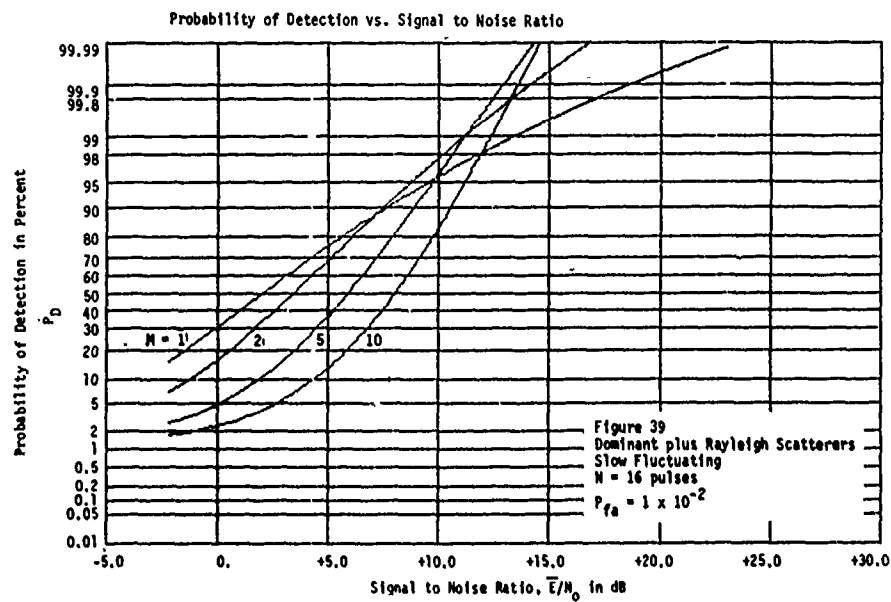
b) For a fast fluctuating target

$$P_{DM} = 1 - \frac{N!}{\left(1 + \frac{\bar{E}}{4MN_0} \right)^N} \gg \sum_{K=0}^N \left(\frac{\bar{E}}{4MN_0} \right)^K I \left[\frac{Y_b}{\left(1 + \frac{\bar{E}}{4MN_0} \right) (\sqrt{N+K})}, N+K-1 \right] \gg \frac{1}{K! (N-K)!} \quad (12).$$

$I[.,.]$ is the incomplete gamma function.

For the slow fluctuating dominant plus Rayleigh target the probability of detection as a function of the signal-to-noise ratio is shown in figures 36, 37, and 38 for $N = 4$ and in figures 39, 40, and 41 for $N = 16$. The different curves for each M do not represent the same scatterer as in the previously discussed Rayleigh case. However they do represent the same overall false alarm probability, P_{fa} , total signal energy, \bar{E} , and number of pulses integrated, N . Since such a target

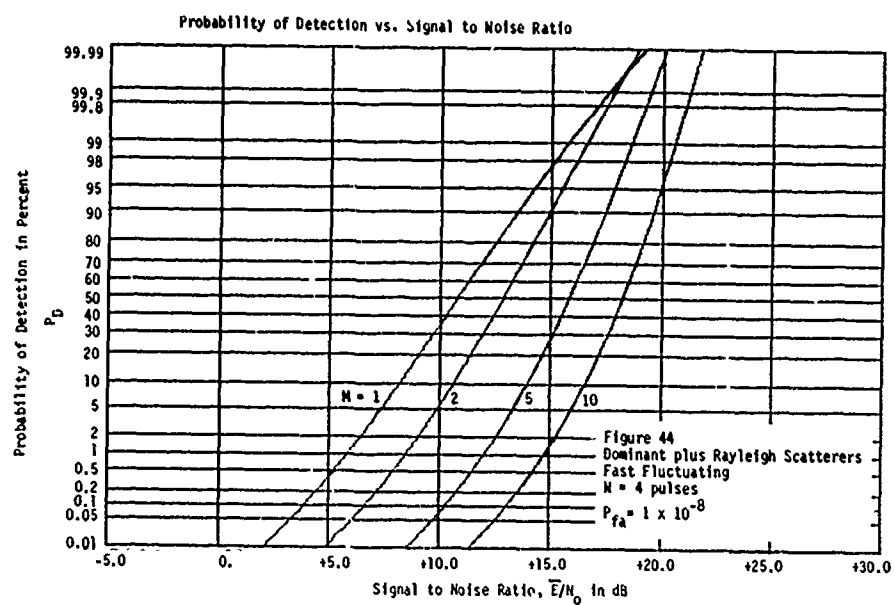
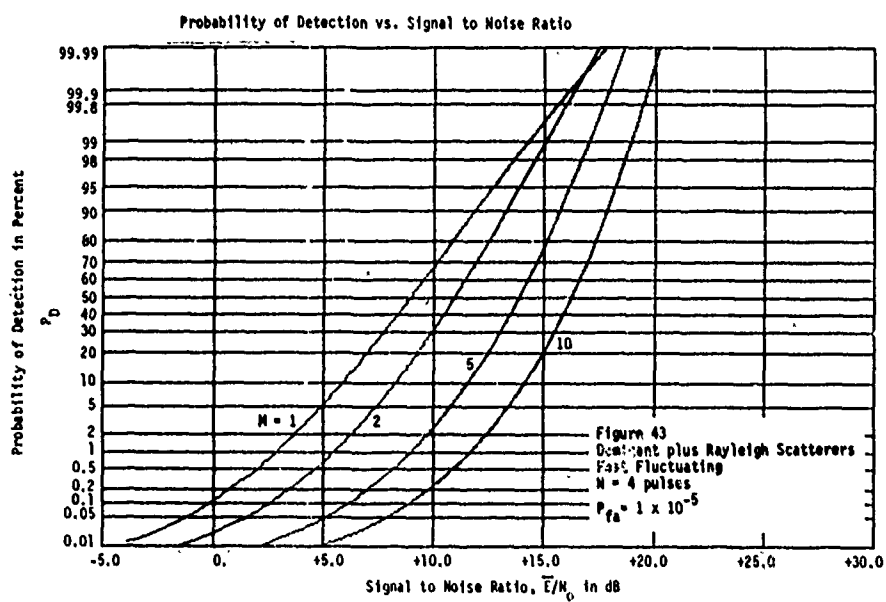
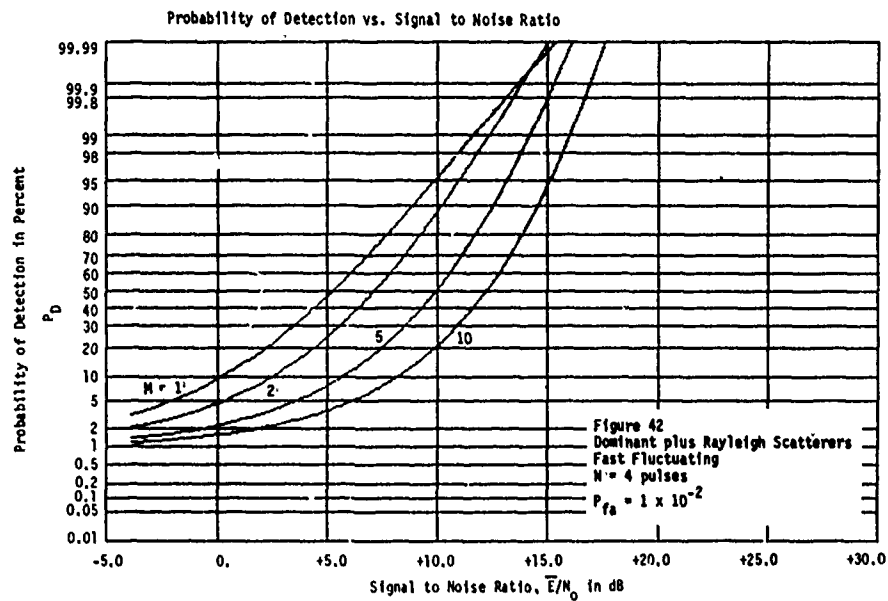


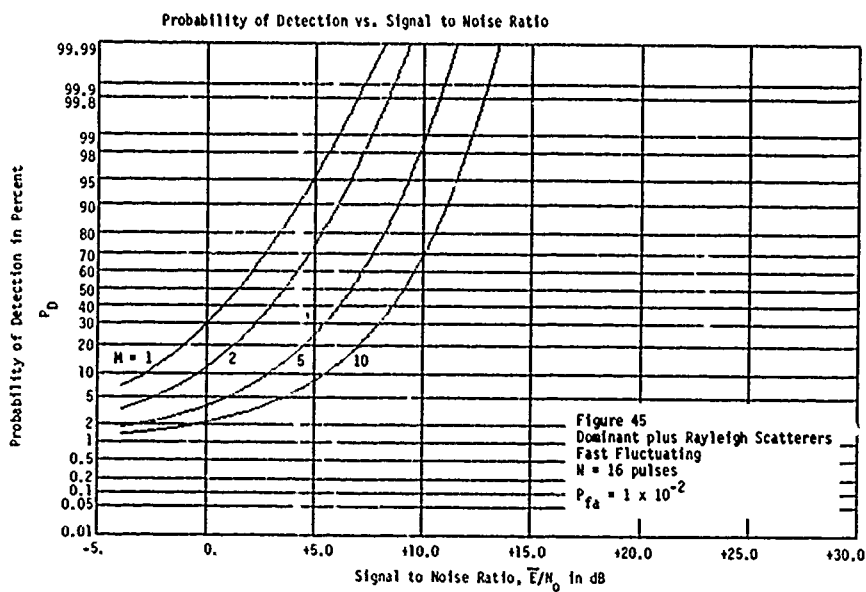
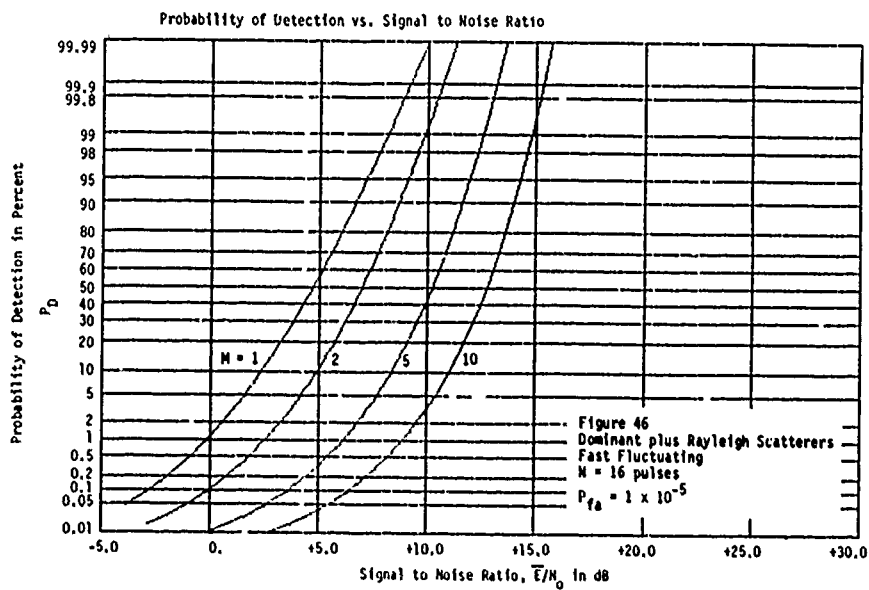
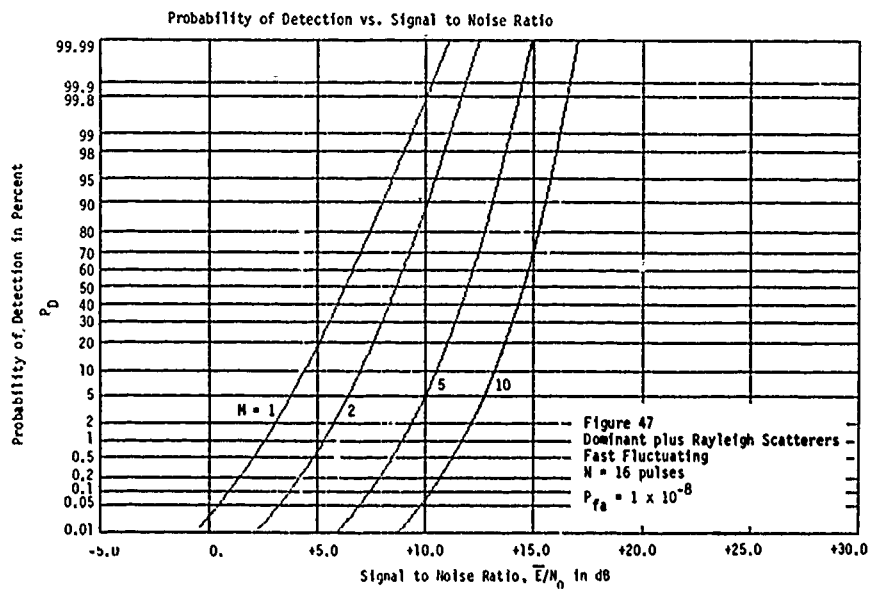


consists of a constant amplitude and a Rayleigh component, the detection performance falls somewhere between that of the constant amplitude scatterer of equation (8) and the Rayleigh slow fluctuating scatterer of equation (9). In figure 36 it is noted that the detection probability increases at a higher rate as the resolution index, M , increases. Above the signal-to-noise ratio of 11.1 dB, maximum performance is obtained for a resolution index of $M = 2$ while above 15.0 dB maximum performance is obtained for $M = 5$. A deterioration in performance is noted with increasing M for low values of signal-to-noise ratio.

For the fast fluctuating dominant plus Rayleigh target the probability of detection as a function of the signal-to-noise ratio is shown in figures 42, 43, and 44 for $N = 4$ and in figures 45, 46, and 47 for $N = 16$. Again the N independent pulse samples result in M constant amplitude estimates at the output of the N pulse integrator. Therefore, the curves for each M represent the same target. In figure 42, where $N = 4$, the detection probability incurs only a slight increase as the resolution index, M , increases. Above the signal-to-noise ratio of 14.2 dB, maximum signal-to-noise ratio is obtained for a resolution index of $M = 2$. In figure 45, where $N = 16$, there is a performance loss for all signal-to-noise ratios with an increase of M .

Note, however, that the same relationships as with the Rayleigh targets hold although not as pronounced. The integrated N dependent pulses from the slow fluctuating target has a higher rate of improvement with signal-to-noise ratio as M increases. Integration of the N



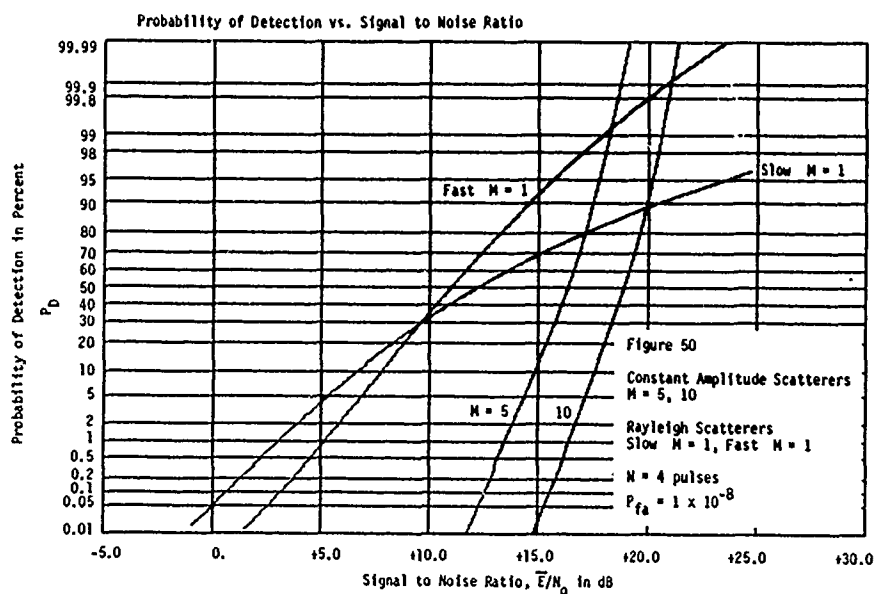
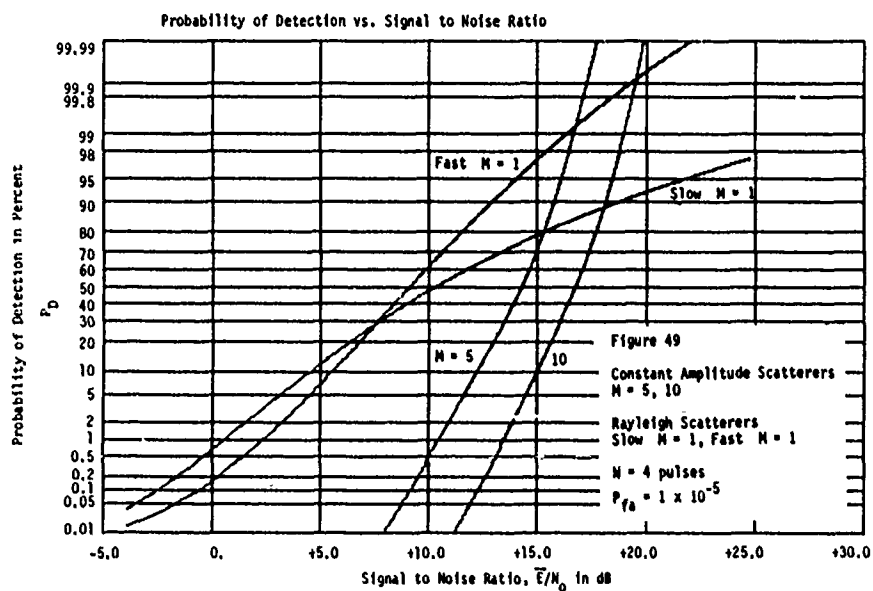
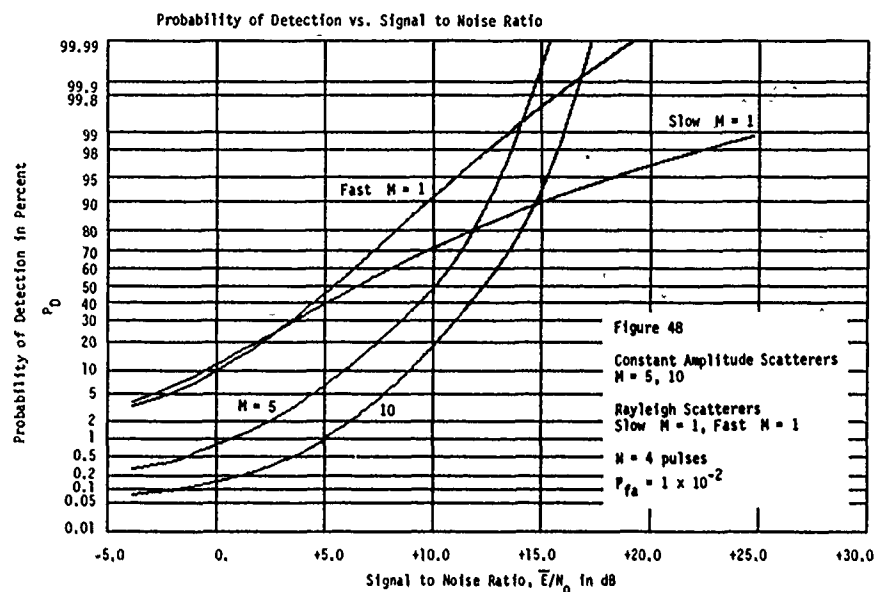


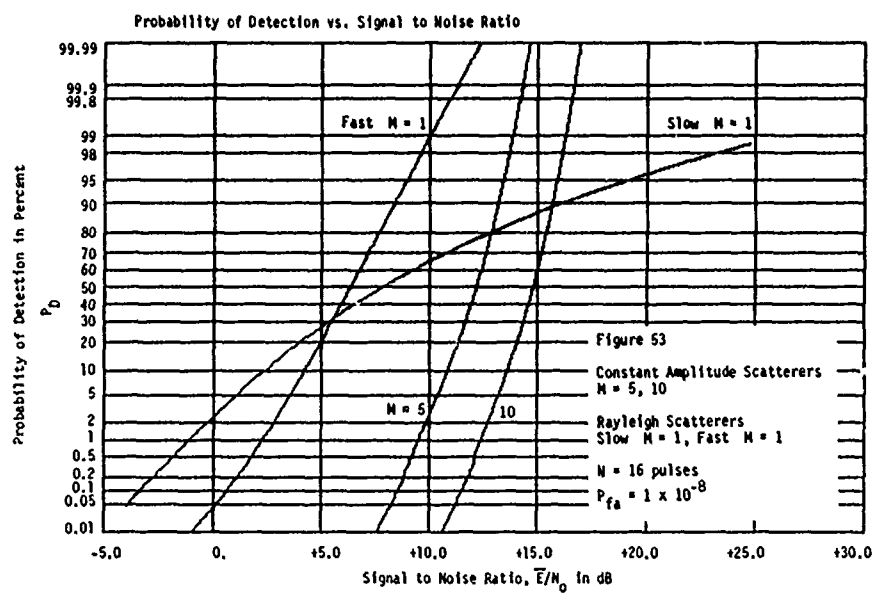
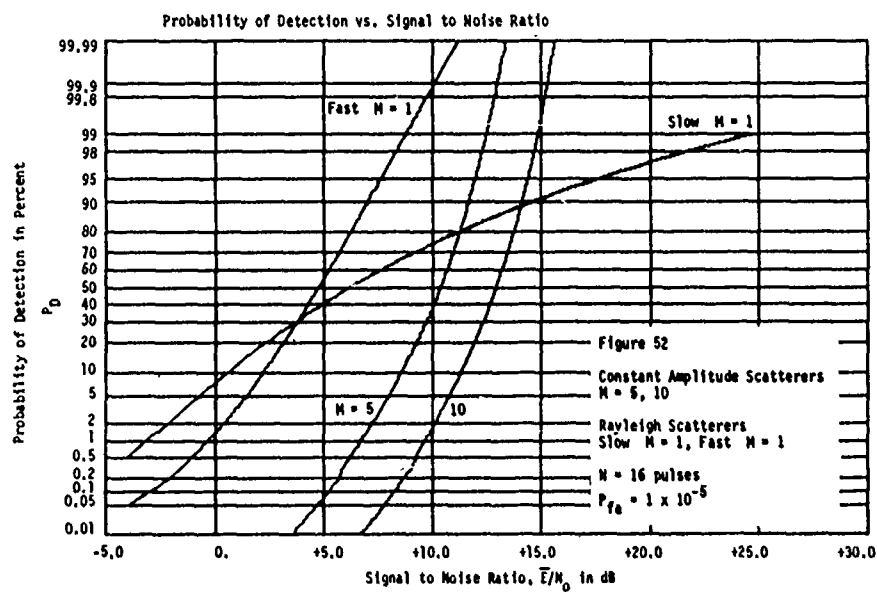
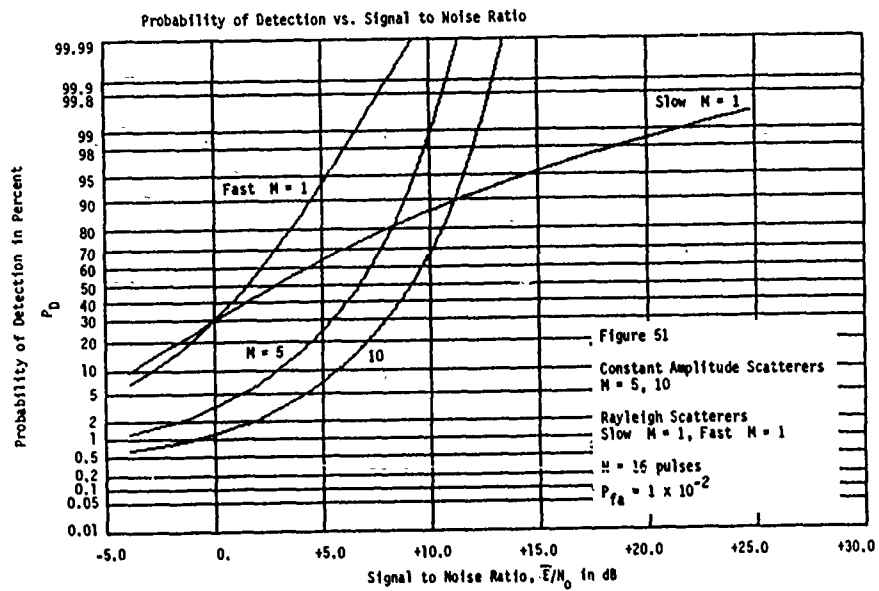
independent pulses from a fast fluctuating target results in an effective performance loss as M increases. Here, as in the Rayleigh fast fluctuating case, the variance of the amplitude estimate decreases with an increase in N , the number of independent samples. Thus for increasing N , the variable $Y(j)$ and performance thereof approaches that of the constant amplitude scatterer when the target is fast fluctuating.

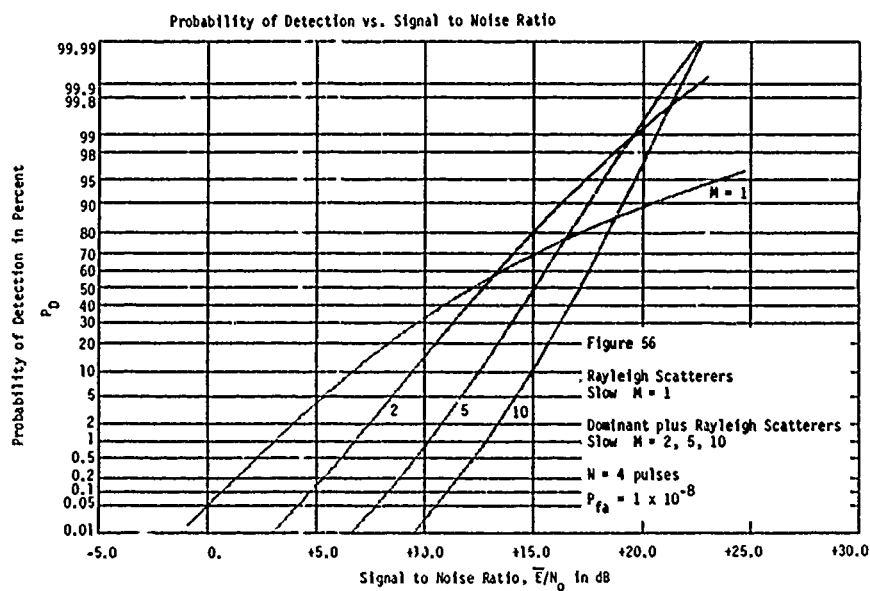
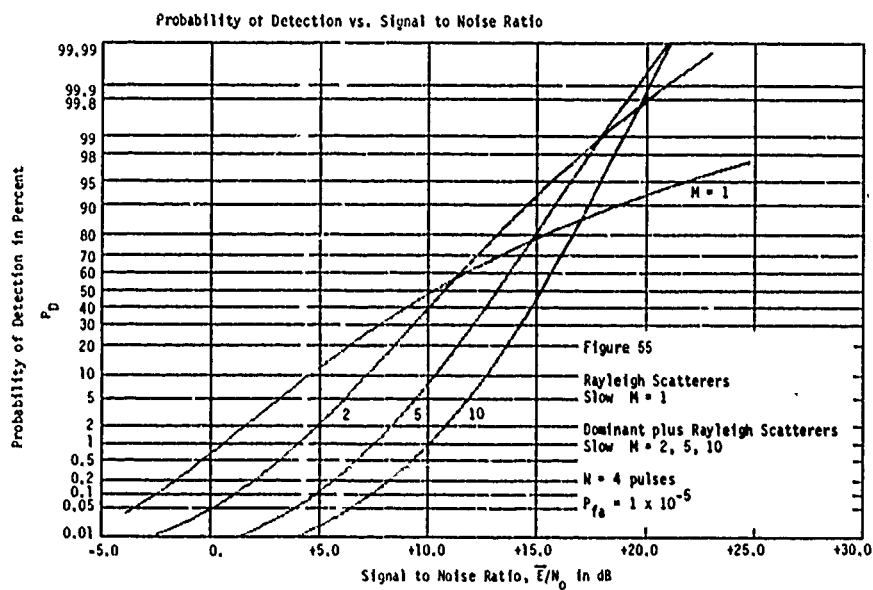
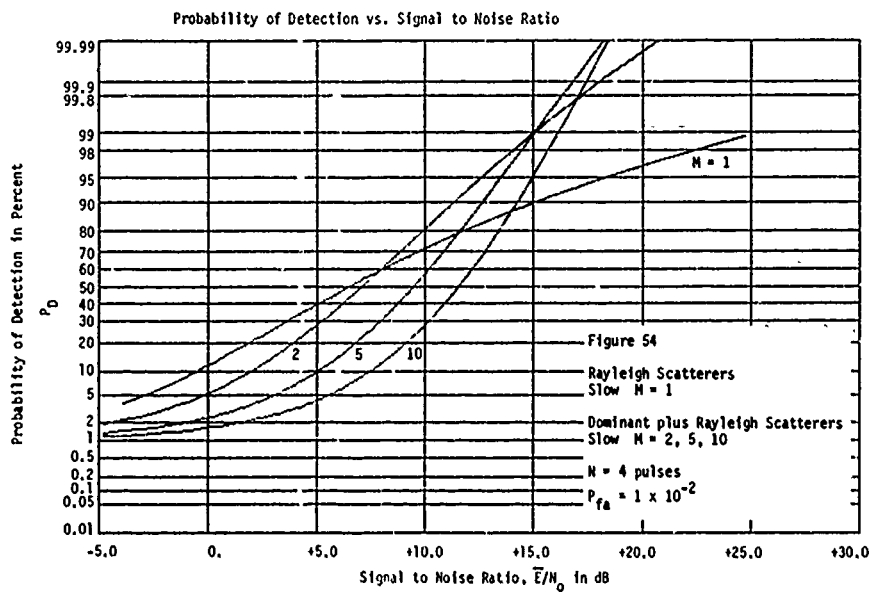
4) Realistic Cases

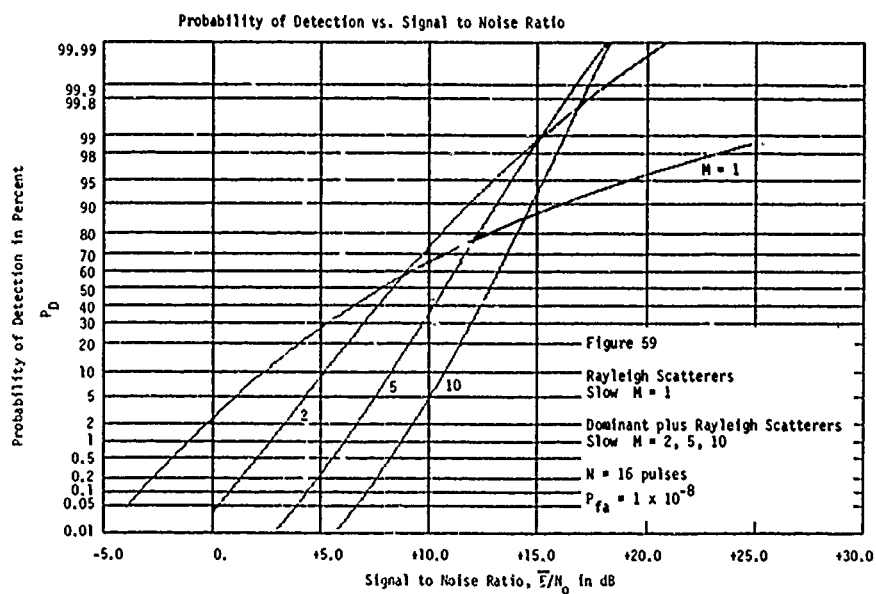
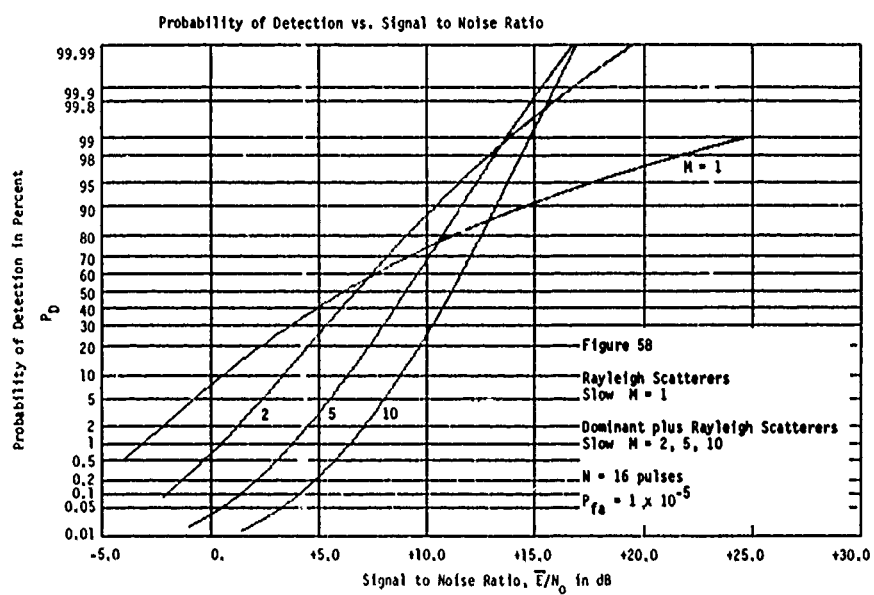
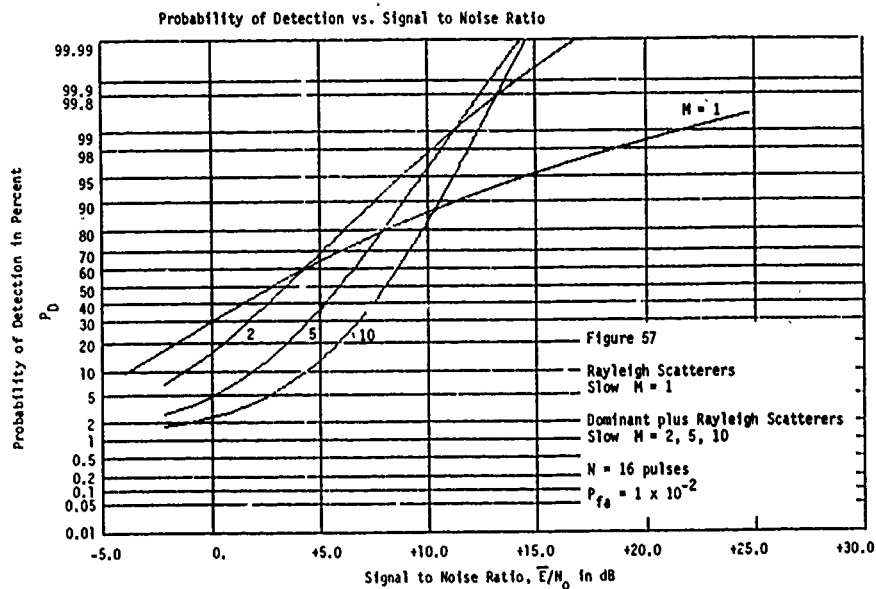
Detection probability curves are shown in figures 48 to 50 for number of pulses, $N = 4$, and in figures 51 to 53 for number of pulses $N = 16$. Performance for the fast and slow Rayleigh fluctuating targets, $M = 1$, is compared with the performance of constant amplitude subscatterers, $M = 5$ and $M = 10$. One can observe the improvement/loss in performance obtained when either a Rayleigh fast or slow fluctuating target is resolved into $M = 5$ and 10 constant scatterer range cells. When this is indeed the scenario, the Rayleigh slow fluctuating target incurs a signal-to-noise improvement as the resolution index, M , increases, the number of pulses, N , increases, and the signal-to-noise ratio is such so that the probability of detection is above 80%. On the other hand, as N increases, a fast fluctuating target is best detected at a resolution index of $M = 1$.

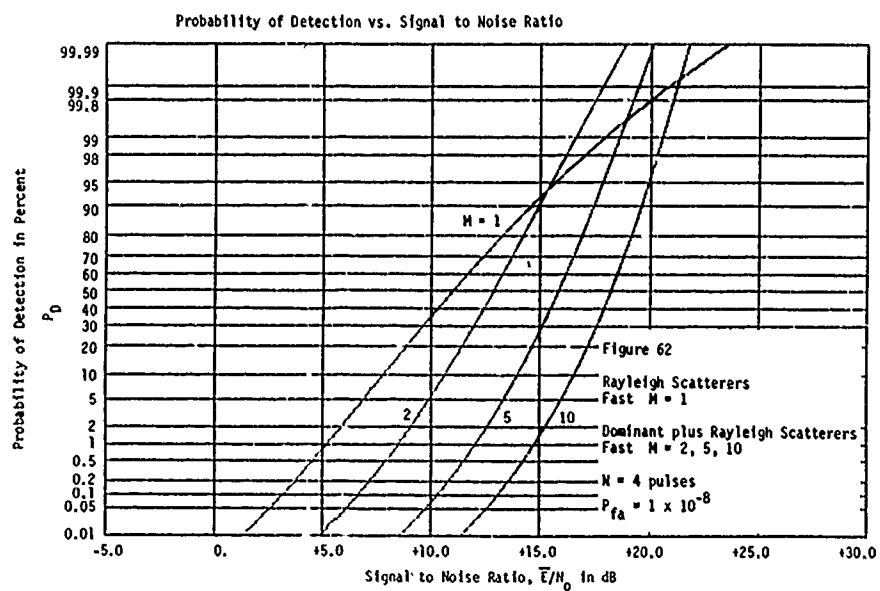
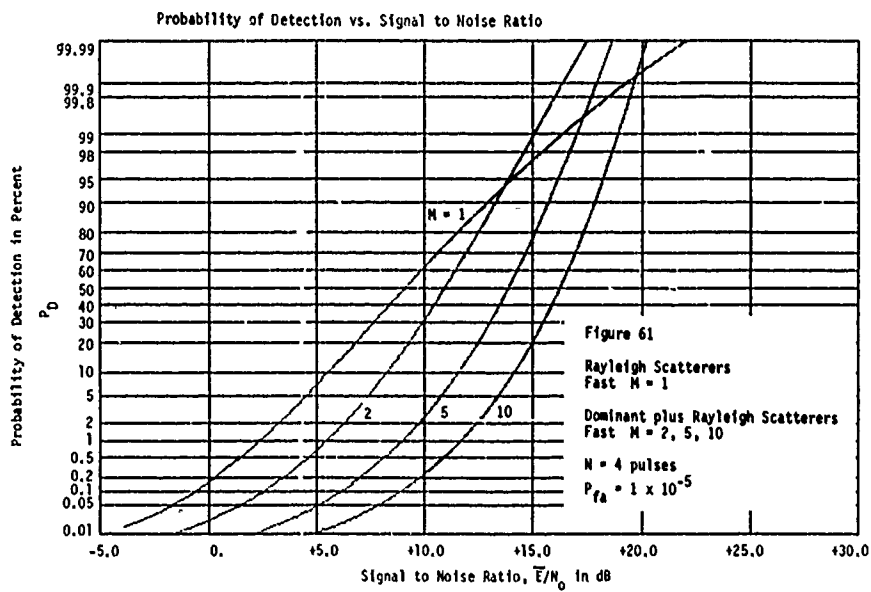
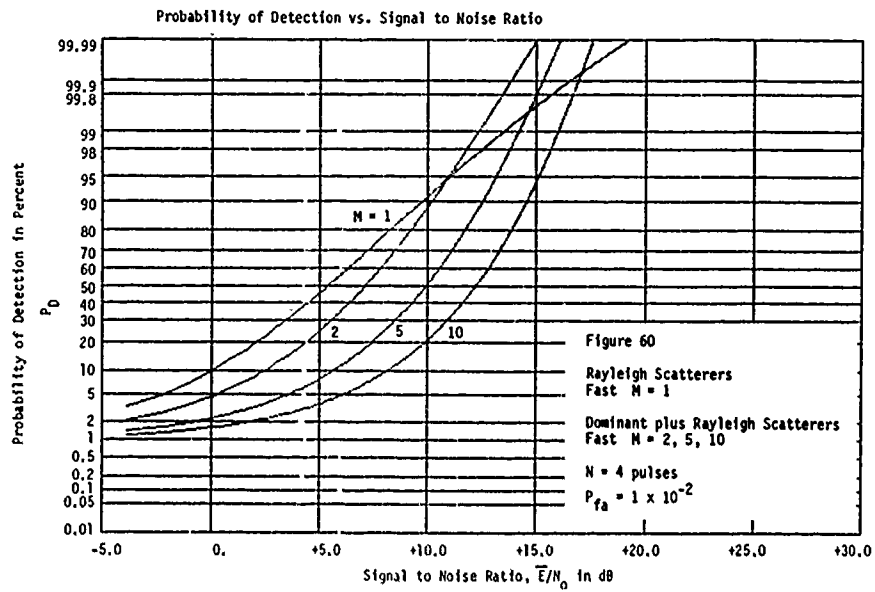
Figures 54 through 59 show detection probability versus signal-to-noise ratio for slow fluctuating Rayleigh targets, i.e. integration of dependent samples. When the slow fluctuating Rayleigh

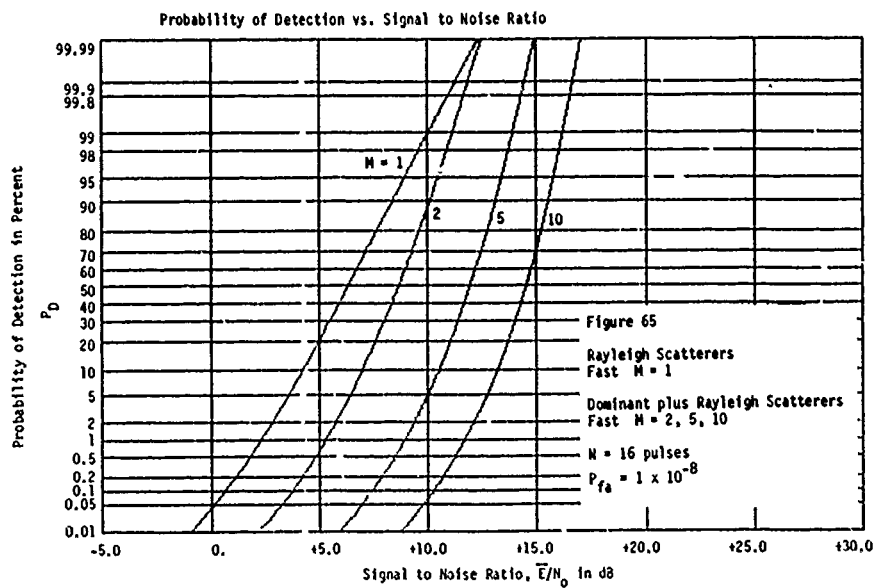
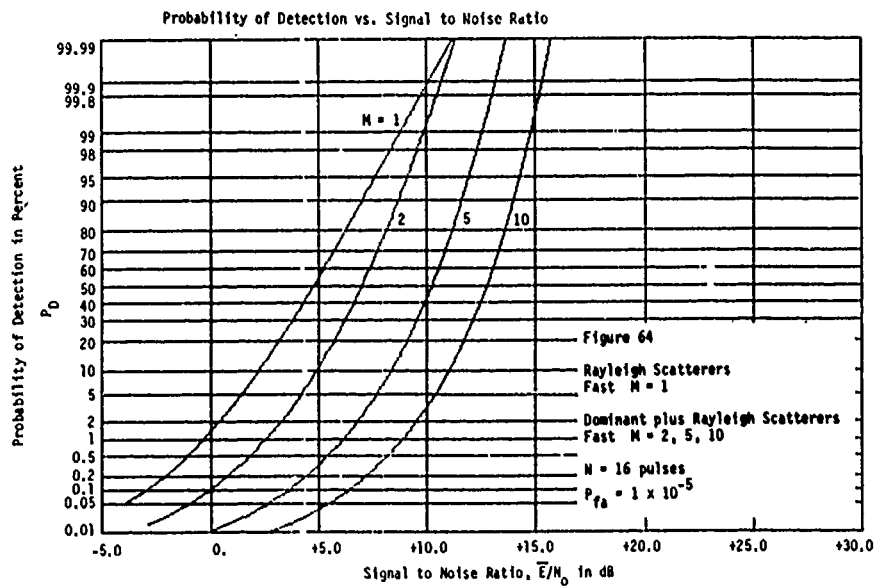
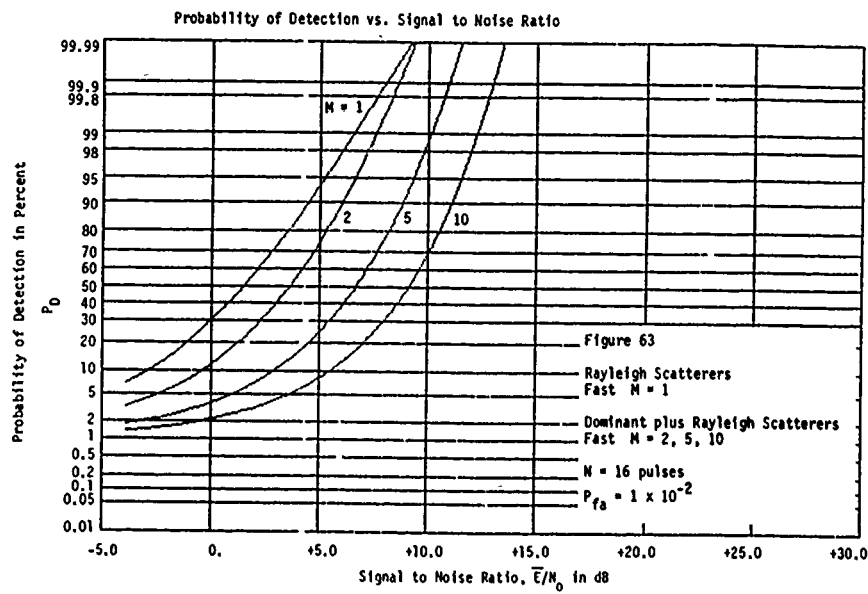












target is resolved into $M = 2, 5, \text{ or } 10$ slow fluctuating dominant plus Rayleigh subscatterers, a signal-to-noise improvement results in much the same manner as resolving into M constant amplitude subscatterers of figures 48 through 53.

In both the above cases, the number of pulses integrated, N , has no effect on the interrelationship (relative shapes) between the various M curves. The assumption that these returns are slow fluctuating renders the improvement/loss with respect to M insensitive to N (since the N samples are dependent). Except for absolute signal energy integration gain, the relative detector performance with respect to M is similar to that of the single pulse case.

Figures 60 through 65 illustrate the manner by which detection performance for fast fluctuating Rayleigh and dominant plus Rayleigh targets converges toward that of constant amplitude targets as the number of pulses, N , increases.

VI. CONCLUSIONS

This work has addressed the detection performance of Rician and Rayleigh models for range-extended targets as suggested in [21]. A summary of the conclusions follow.

For high signal-to-noise ratios:

- o Fast fluctuating Rayleigh targets used in conjunction with large N pulse waveforms incur a performance degradation as the number of range cells, M, increases to the point at which the individual subscatterers are resolved.
- o Single pulse fast fluctuating Rayleigh targets, in conjunction with small-N pulse waveforms, and slow fluctuating Rayleigh targets, with any N, incur a performance improvement as the number of range cells, M, increases to the point at which the individual subscatterers are resolved.

For low signal-to-noise ratios:

- o The best detection performance is achieved at $M = 1$, i.e. the entire target occupies one single range resolution cell. This applies for any scatterer model.

When these procedures are applied to distributed clutter, the total false alarm count may increase or decrease depending on the statistical properties of the clutter. Just as the Rayleigh slow fluctuating target incurs an increase in detection probability with increased range resolution, so would Rayleigh slow fluctuating clutter incur a higher false alarm count (given a similar threshold adjustment for constant false alarm due to thermal noise) over the same range span.

APPENDIX A

Development of the Gram-Charlier Series for Detection Probability of Constant Amplitude Scatterers

A search was made to determine analytical expressions/expansions for the detection probability of constant targets in noise; the incomplete Toronto function or as sometimes denoted Marcum's Q function. No suitable expansion was found that could be readily programmed. It was decided to undertake a fourth-order Gram-Charlier series approximation. The data generated from these approximations was verified and found to be well within the accuracy of the curves appearing in published literature.

The Gram-Charlier series expansion is given by

$$p(x) = \frac{1}{\sigma} \sum_{i=0}^{\infty} c_i \phi^{(i)}\left(\frac{x - \bar{x}}{\sigma}\right) \quad (A-1)$$

where $\phi^{(0)}(x) = \phi(x) = \left(\frac{1}{\sqrt{2\pi}}\right) \exp\left(-\frac{x^2}{2}\right)$

and $\phi^{(i)}(x) = \frac{d^i \phi(x)}{dx^i}$

and where $p(x)$ is the approximated probability density function. Using the procedure given in [5] we may determine the coefficients c_i as follows.

First we determine the moments from the characteristic function of Y

$$m_n = \frac{1}{j^n} C_Y^{(n)}(0)$$

where m_n is the n th moment of the distribution of Y and $C_Y^{(n)}(0)$ is the n th derivative of the characteristic function $C_Y(\xi)$ evaluated at $\xi = 0$. For the particular case of interest, i.e. the constant scatterer in Gaussian noise, the characteristic function $C_Y(\xi; R_p)$ of Y is

$$\begin{aligned} C_Y(\xi; R_p) &= \prod_{i=1}^N \left(\frac{1}{1 - j\xi} \right) \exp\left(\frac{jR_p \xi}{2(1-j\xi)} \right) \\ &= \frac{1}{(1 - j\xi)^N} \exp\left(\frac{jNR_p \xi}{2(1-j\xi)} \right) \end{aligned}$$

R_p is equal to $2\bar{E}/MN_0$. In the constant amplitude case, $\bar{E} = E$. The first derivative of $C_Y(\xi; R_p)$ is

$$\begin{aligned} \frac{d C_Y(\xi; R_p)}{d\xi} &= \frac{jNR_p}{2(1-j\xi)^{N+2}} \exp\left(\frac{j\xi NR_p}{2(1-j\xi)} \right) + \\ &\quad \frac{jN}{(1-j\xi)^{N+1}} \exp\left(\frac{j\xi NR_p}{2(1-j\xi)} \right) \end{aligned}$$

Evaluating m_1 yields

$$m_1 = \bar{Y} = (N R_p / 2) + N$$

In a similar manner the second and third moments are:

$$m_2 = (N R_p / 2)^2 + 2(N R_p / 2)(N+1) + N(N+1)$$

$$m_3 = (N R_p / 2)^3 + 3(N R_p / 2)^2(N+2) + 3(N R_p / 2)(N+1)(N+2) + N(N+1)(N+2)$$

Coefficients c_i can be evaluated with the relation

$$c_i = \frac{(-1)^i}{i!} \int_{-\infty}^{+\infty} p(x) H_i\left(\frac{x - \bar{x}}{\sigma}\right) dx$$

where the first four Hermite polynomials are

$$H_0(x) = 1$$

$$H_1(x) = x$$

$$H_2(x) = x^2 - 1$$

$$H_3(x) = x^3 - 3x$$

Evaluating the above integral yields

$$c_0 = 1$$

$$c_1 = c_2 = 0$$

$$c_3 = -\left(\frac{\alpha_3}{3!}\right)$$

where α_i is the i th central moment of $p(x)$ normalized by σ^i :

$$\alpha_i = \frac{1}{\sigma^i} \int_{-\infty}^{+\infty} (x - \bar{x})^i p(x) dx$$

Since
$$m_n = \int_{-\infty}^{+\infty} x^n p(x) dx$$

then
$$\alpha_3 = (m_3 - 3m_2m_1 + 2m_1^3) / \sigma^3$$

where
$$\sigma^2 = m_2 - m_1^2$$

The order of magnitude of coefficient c_i does not decrease uniformly as i increases. The Edgeworth series is yielded by regrouping the terms of the Gram-Charlier series with the same magnitude. The hierarchy of terms in descending order of magnitude is

$$\begin{aligned} i &= 0 \\ i &= 3 \\ i &= 4, 6 \\ i &= 5, 7, 9 \end{aligned}$$

A fourth-order approximation of $p(x)$ is generated by expanding the first four terms of the Gram-Charlier series, i.e. $i = 0, 1, 2, 3$. Upon substitution of all the above terms into equation (A-1) we have for the fourth-order probability density function

$$p(x) = \frac{1}{\sqrt{2\pi}} [c_0 - c_3(x^3 - 3x)] \exp\left(-\frac{x^2}{2}\right)$$

The detection probability is obtained from the integral

$$P_{DM} = \int_{x=x_b}^{\infty} p(x) dx$$

$$P_{DM} = \frac{1}{\sqrt{2\Pi}} \int_{x_b=(Y_b-\bar{Y})/\sigma}^{\infty} [c_0 - c_3(x^3 - 3x)] \exp\left(-\frac{x^2}{2}\right) dx$$

$$P_{DM} = \frac{1}{2} \operatorname{erfc}(x_b / \sqrt{2}) + c_3 \left(\frac{1}{\sqrt{2\Pi}} \right) \left(1 - x_b^2 \right) \exp\left(-\frac{x_b^2}{2}\right)$$

$$\text{where } \operatorname{erfc}(x_b / \sqrt{2}) = 2 \int_{x=x_b}^{\infty} \left(\frac{1}{\sqrt{2\Pi}} \right) \exp\left(-\frac{x^2}{2}\right) dx$$

is the complimentary error function. The error function is readily evaluated by a series expansion. (3)

$$\operatorname{erf}(z) = 1 - \operatorname{erfc}(z) = \frac{2}{\sqrt{\Pi}} \sum_{n=0}^{\infty} \frac{(-1)^n z^{2n+1}}{n! (2n+1)}$$

Also $\operatorname{erf}(-z) = -\operatorname{erf}(+z)$

(3)

See this reference for information about the error function.
 "Handbook of Mathematical Functions," U.S. Department of
 Commerce, National Bureau of Standards, AMS 55, June 1964.

APPENDIX B

The Incomplete Toronto Function

The integral

$$T_B(m,n,r) = 2 r^{n-m+1} \exp(-r^2) \int_0^B t^{m-n} \exp(-t^2) I_n(2rt) dt \quad (B-1)$$

is called the "Incomplete Toronto Function". In the above integral $I_n(x)$ denotes the modified Bessel function of the first kind and of order n .

An application of this function is in the expression for the probability of declaring that the signal s_i is present (H_1 hypothesis). The observation under the two hypothesis is

$$v_i = n_i \quad : \quad H_0$$

$$v_i = s_i + n_i \quad : \quad H_1$$

for $i = 1, 2, 3, \dots, N$. The n_i are complex Gaussian, zero mean, and variance of N_0 . The s_i are constant amplitude, \bar{E} , with uniform phase: $-\pi < \theta_i < +\pi$.

A likelihood ratio test for the above hypothesis leads to the following decision rule:

$$Y \underset{H_0}{\overset{H_1}{\geq}} Y_b$$

where

$$Y = \frac{1}{2} \sum_{i=1}^N |v_i|^2 \quad (B-2)$$

and Y_b is a threshold which establishes the boundary and the critical region.

The probability density function of Y given \bar{E} and given N_0 is

$$p(Y:R_p) = (2Y/NR_p)^{(N-1)/2} \exp(-Y - NR_p/2) I_{N-1}(\sqrt{2NR_p Y}) : Y \geq 0$$

$$= 0 : \text{Otherwise.}$$

(B-3)

where $I_{N-1}(x)$ is the modified Bessel function of the first kind, of order $N-1$, and $R_p = 2\bar{E}/N_0$. (4) For the constant amplitude case, $\bar{E} = E$. The probability that $Y \geq Y_b$, i.e. the critical region, is the cumulative density function

$$P_d = \int_{Y_b}^{\infty} (2Y/NR_p)^{(N-1)/2} \exp(-Y - NR_p/2) I_{N-1}(\sqrt{2NR_p Y}) dY$$

(B-4)

(4)

For simplicity we confine the discussion to a single scatterer and avoid any association with over resolved targets, thus reference to resolution index, M , has been omitted.

This integral is of the form of equation (B-1). We may express P_d in terms of the incomplete Toronto function.

$$P_d = 1 - T_{\sqrt{Y_b}}(2N-1, N-1, \sqrt{NR_p/2}) \quad (B-5)$$

This is the probability that the H_0 hypothesis will be rejected or equivalently, that the constant amplitude signal will be detected.

An approximation to equation (B-5) may be obtained using a Gram-Charlier series. A four term approximation is as follows.

$$P_d = \frac{1}{2} \operatorname{erfc}(x_b / \sqrt{2}) + c_3 \left(\frac{1}{\sqrt{2\pi}} \right) (1 - x_b^2) \exp\left(-\frac{x_b^2}{2}\right)$$

$$\text{where } \operatorname{erfc}(x_b / \sqrt{2}) = 2 \int_{x=x_b}^{\infty} \left(\frac{1}{\sqrt{2\pi}} \right) \exp\left(-\frac{x^2}{2}\right) dx$$

is the complimentary error function.

ACKNOWLEDGMENT

The authors wish to acknowledge James H. Michels of Rome Air Development Center for his review and constructive comments on the subject matter of this paper.

REFERENCES

- [1] Woodward, P. M., "Probability and Information Theory with Applications to Radar," McGraw-Hill, New York, 1953.
- [2] Swerling, P., "Probability of Detection for Fluctuating Targets," Rand Research Memo RM-1217, March 1954. Also reissued in IRE Trans. on Info. Theory, vol. IT-6, no. 2, pp. 269-308, April 1960.
- [3] Marcum, J. I., "A Statistical Theory of Target Detection by Pulsed Radar," Rand Research Memo RM-754, December 1947. Also reissued in IRE Trans. on Info. Theory, vol. IT-6, no. 2, pp. 59-144, April 1960.
- [4] Marcum, J. I., "A Statistical Theory of Target Detection by Pulsed Radar (Mathematical Appendix)," Rand Research Memo RM-753, July 1948. Also reissued in IRE Trans. on Info. Theory, vol. IT-6, no. 2, pp. 145-267, April 1960.
- [5] DiFranco, J. V., and Rubin, W. L., "Radar Detection," Prentice-Hall, Inc., Englewood Cliffs, New Jersey, 1968.
- [6] North, D. O., "An Analysis of the Factors Which Determine Signal/Noise Discrimination in Pulsed-Carrier Systems," RCA Labs Tech Rept. PTR-6C, June 25, 1943. Also reissued in Proc. IEEE, vol. 51, no. 7, pp. 1015-1027, July 1963.
- [7] Blake, L. V., in Discussion on "The Statistical Properties of Noise Applied to Radar-Range Performance," Proc. IRE, vol. 40, no. 4, pp. 487-489, April 1952.
- [8] Miller, K. S., and Bernstein, R. I., "An Analysis of Coherent Integration and Its Application to Signal Detection," IRE Trans. on Info. Theory, vol. IT-3, no. 4, pp. 237-248, December 1957.
- [9] Barton, D. K., "Frequency Agility and Diversity," Radars, Volume 6, Artech House, Inc., Dedham, Mass., 1977.

- [10] Dana, R. A., and Moraitis, D., "Probability of Detecting a Swerling I Target on Two Correlated Observations," IEEE Trans. on Aerosp. and Electron. Sys., vol. AES-17, no. 5, pp. 727-730, September 1981.
- [11] Finn, H. M., "A New Approach to Sequential Detection in Phased Array Radar Systems," Proc. Nat. Winter Conv. on Mil. Elect., IEEE 1963, vol. II, pp. 4-3 to 4-12.
- [12] Marcus, M. B., and Swerling, P., "Sequential Detection in Radar with Multiple Resolution Elements," IRE Trans. on Info. Theory, vol. IT-8, no. 3, pp. 237-245, April 1962.
- [13] Helstrom, C. W., "A Range-Sampled Sequential Detection System," IRE Trans. on Info. Theory, vol. IT-8, no. 1, pp. 43-47, January 1962.
- [14] Preston, G. W., "The Search Efficiency of the Probability Ratio Sequential Search Radar," IRE Conv. Rec. 60, Pt. 4, pp. 116-124.
- [15] Nitzberg, R., "Effect of a Few Dominant Specular Reflectors Target Model Upon Target Detection," IEEE Trans. on Aerosp. and Electron. Sys., vol. AES-14, no. 4, pp. 670-673, July 1978.
- [16] Hughes II, P. K., "A High-Resolution Radar Detection Strategy," IEEE Trans. on Aerosp. and Electron. Sys., vol. AES-19, no. 5, pp. 663-667, September 1983.
- [17] Skolnik, M. I., "Introduction to Radar Systems," McGraw-Hill, Inc., 1980.
- [18] Heatley, A. H., "A Short Table of the Toronto Functions," Trans. Roy. Soc. Canada, 37 (Sec. III), pp. 13-29, 1943.
- [19] Fehlner, L. F., "Marcus's and Swerling's Data on Target Detection by a Pulsed Radar," Report TG-451, Applied Physics Laboratory, John Hopkins University, Silver Spring, Maryland, July 1962.

- [20] Fehlner, L. F., "Supplement to Marcum's and Swerling's Data on Target Detection by a Pulsed Radar," Report TG-451A, Applied Physics Laboratory, John Hopkins University, Silver Spring, Maryland, September 1964.
- [21] Swerling, P., "Recent Developments in Target Models for Radar Detection Analysis," Technology Service Corp., Santa Monica, California. Presented at AGARD Avionics Technical Symposium on 'Advanced Radar Systems', May 1970.

SUPPLEMENTARY

INFORMATION



DEPARTMENT OF THE AIR FORCE
ROME LABORATORY (AFSC)
GRIFFISS AIR FORCE BASE, NEW YORK 13441-5700

1

ERRATA

REPLY TO
ATTN OF:

IMPS/587-2628

B089 870

18 Jun 92

SUBJECT:

Change of Distribution Limitation

TO:

DTIC-EDAC

OCD

1. According to DOD Directive 5230.24, the following Rome Laboratory ~~technical report has been changed from limited to unlimited~~ (releasable to the public):

RADC-TR-84-61 dated Sep 84 (AD-B089 870)

2. ~~Subject document may now be released to the National Technical Information Service (NTIS)~~

3. If you have any questions, please contact the undersigned at DSN 587-2628.

Shirley A. Lyons

SHIRLEY A. LYONS, STINFO Officer
STINFO Office

Cy to: RL/IMD
/INF
/SUL

ERRATA

ERRATA:

B089 870

FL-7 RL/IMPS Jun 92